

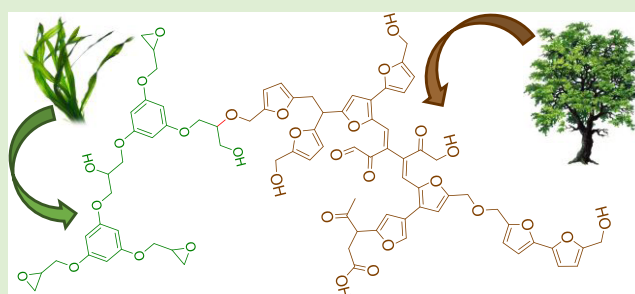
# Biorefinery Byproducts and Epoxy Biorenewable Monomers: A Structural Elucidation of Humins and Triglycidyl Ether of Phloroglucinol Cross-Linking

Cristina Cantarutti, Roxana Dinu, and Alice Mija\*<sup>✉</sup>

Institut de Chimie de Nice, UMR CNRS 7272, Université Côte d'Azur, Université Nice-Sophia Antipolis, 06108 Nice Cedex 02, France

## S Supporting Information

**ABSTRACT:** The need for thermosets from renewable resources is continuously increasing to find eco-friendly alternatives to petroleum-derived materials. Products obtained from biomass have shown to play an important role in this challenge. Here, we present the structural characterization of new biobased thermosets made of humins, a byproduct of lignocellulosic biorefinery, and glycidylated phloroglucinol coming from the biomass phenolic fraction. By employing attenuated total reflection-Fourier transform infrared and NMR spectroscopies, we elucidated the connections between these two systems, contributing to clarify their molecular structures and their reactivities. We demonstrated that the resin curing takes place through ether bond formation between humin hydroxyl functions and phloroglucinol epoxides. Besides cross-linking, humins show a complex rearrangement of their furanic structure through different concomitant chemical pathways depending on the reaction conditions.



resin curing takes place through ether bond formation between humin hydroxyl functions and phloroglucinol epoxides. Besides cross-linking, humins show a complex rearrangement of their furanic structure through different concomitant chemical pathways depending on the reaction conditions.

## INTRODUCTION

The production of novel eco-compatible materials from natural sources that can replace harmful petroleum-based materials is becoming an urgent issue. By developing materials using biodegradable and renewable components, it will be possible to reduce the human impact on the environment and the dependence on nonrenewable fossil resources.<sup>1</sup> Lignocellulosic biomass demonstrated to be an ideal candidate for this purpose.<sup>2–4</sup> In particular, humins are emerging as promising starting materials for polymeric material preparation.<sup>5–8</sup> Humins are the insoluble viscous polymeric fraction that is formed during the acid-catalyzed dehydration (ACD) of sugars obtained from lignocellulosic biomass. This process leads to the production of high-value chemicals like 5-hydroxymethylfurfural (HMF) and levulinic acid. However, uncontrollable condensation cannot be avoided and leads to humin formation.<sup>9–13</sup> Instead of considering humins as a waste, a new approach aimed at their valorization encouraged by the first results showing their great potential in materials chemistry is attracting increasing attention. One of the main critical issues regarding the humins is their molecular structure. Many different formation routes and structures have been proposed (Figure 1), but a definitive model has not yet been established.

A pathway that assumes a HMF polycondensation through electrophilic substitution entailing the formation of ether and acetal bonds between furanic rings was proposed by Summerskii et al.<sup>14</sup> They found that humins are made up by 60% furan rings and 20% aliphatic chains. Another group suggested that the product of HMF rehydration, i.e., 2,5-dioxo-6-hydroxyhexanal

(DHH), is a key intermediate in humin formation. In this perspective, DHH and HMF carbonyls undergo aldol condensation leading to humins.<sup>15,17</sup>

Moreover, the presence of carbonyl groups was ascertained and quantified as 6.6 wt %.<sup>18</sup> Humins can be produced also by hydrothermal carbonization (HTC) processes, which do not involve acidic conditions.<sup>19,20</sup> The humins produced by HTC have a different structure, but they can be isolated and purified easily; therefore, much more efforts were focused on their structural characterization.<sup>21–24</sup> HTC humins were found to contain furan fragments linked through aliphatic groups at the  $\alpha$  and  $\beta$  positions and oxygenated functional groups (alcohols, ketones, aldehydes, and acids).<sup>16,25–27</sup> In particular, van Zandvoort et al.<sup>16</sup> showed by carbon solid-state NMR the linkages between furanic  $C_\alpha$  and aliphatic carbons and between  $C_\alpha-C_\alpha$ . The authors found that furanic  $C_\beta$  contributes only in minimal parts to the humin network formation. In addition, in their study, the content of oxygenated groups was found to be very low and no clear evidence for aldehyde presence was found. However, industrial humins are more complex and heterogeneous materials. A new approach for the valorization of humins is to use them for new biobased thermosets and composite materials. Humins have shown to enhance the modulus and the tensile strength of pure polyfurfuryl alcohol, giving stronger resins.<sup>5</sup> In addition to the technological improvement of the

Received: September 9, 2019

Revised: October 29, 2019

Published: November 1, 2019

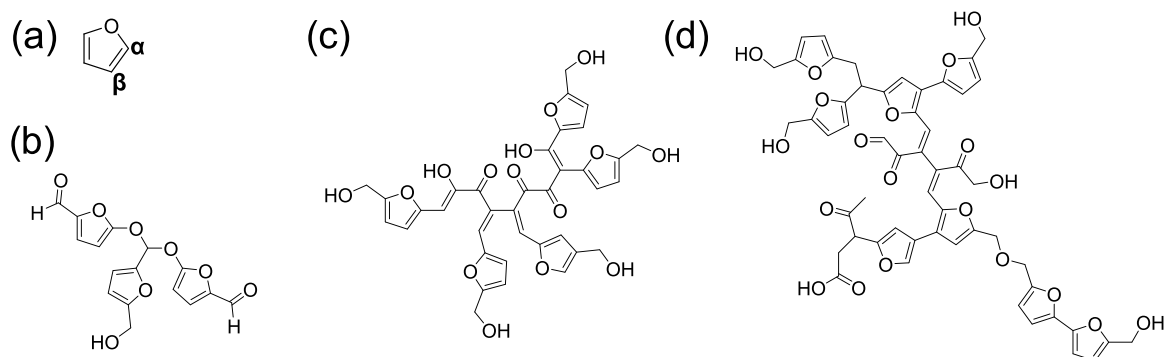


**Figure 1.** (a) Labeling scheme for the furan fragment. Humin structures proposed by (b) Sumerskii et al.,<sup>14</sup> (c) by Patil and Lund,<sup>15</sup> and (d) by van Zandvoort et al.<sup>16</sup>

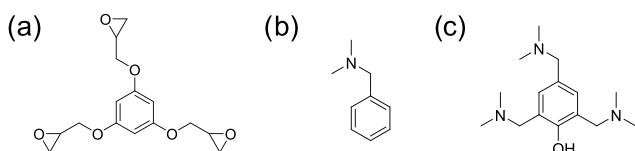


**Figure 2.** Structures of (a) TGPh, (b) BDMA, and (c) accelerator.

resulting materials, the lower cost of humins and their renewable character are not negligible advantages. However, insights into the changes that occur in the structure of humins upon their valorization are still poor, mainly because of the complexity of their structure. Understanding their complex modifications and their reactivity would greatly improve their valorization.

In this work, humins derived from biorefinery acid-catalyzed dehydration processes were combined with triglycidyl ether of phloroglucinol (TGPh) in the presence of (*N,N*-benzyl-dimethylamine) (BDMA) as the basic catalyst and/or 2,4,6-tris(dimethylaminomethyl)phenol (referred to as the accelerator) as the curing accelerator (Figure 2).

The product of the copolymerization reaction was characterized from a structural point of view with attenuated total reflection (ATR)-Fourier transform infrared (FTIR) and NMR spectroscopies. TGPh is a biobased aromatic epoxy monomer obtained from phloroglucinol, which is extracted from algae.<sup>28</sup> Epoxy polymers are widely employed thermosetting materials characterized by good adhesion properties, good chemical resistance, and excellent thermal and mechanical properties. Many epoxies employed for material purposes are slightly modified by the addition of a carbon to the oxirane ring, giving the so-called glycidyl group. In addition, aromatic compounds confer more toughness, stiffness, and temperature stability to the final material thanks to  $\pi$ -stackings. Nowadays, most of the epoxy resins are obtained from diglycidyl ether of bisphenol A (DGEBA), which is a petrol-based molecule. Bisphenol A (BPA) has been classified as a carcinogen, mutagen, and reprotoxic substance, and it is recognized as an endocrine disruptor.<sup>29–32</sup> Since it can be released from epoxy thermosets through hydrolysis, the necessity to replace it in material preparation is becoming a compelling goal. The use of biobased epoxy polymers in place of DGEBA brings the double advantage of BPA replacement and of using renewable resources. For these reasons, a biosourcing epoxy polymer like TGPh was chosen for humin-based thermoset preparation. The most common curing agents for epoxy resins are amines and especially tertiary amines.<sup>33–35</sup> Tertiary amines are Lewis bases that are added to epoxy monomers in small nonstoichiometric amounts acting as true catalysts by initiating a self-propagating anionic polymerization through

the opening of the oxirane ring (Scheme 1). The resulting polymer is a polyether whose ether bonds are thermally stable and are stable also toward most acids and alkalies. The mechanism of the ring opening can proceed by either bimolecular nucleophilic substitution ( $S_N2$ ) or unimolecular nucleophilic substitution ( $S_N1$ ), depending on the nature of the epoxide and on the reaction conditions. When the epoxide is asymmetric, two different regioisomers can be formed. Under basic conditions, ring opening occurs mainly by an  $S_N2$  mechanism, and the less substituted carbon is the site of nucleophilic attack. In acidic conditions, the mechanism is substantially an  $S_N1$  and the nucleophile attacks the more substituted carbon because it can better accommodate the positive charge (more stable carbocation).

To improve the reactivity of epoxy resins with tertiary amine curing agents, often a hydroxyl-containing, especially phenolic, species is added.<sup>36,37</sup> Under basic conditions, the phenolic group can be deprotonated and open the epoxide, favoring the polymerization propagation. In the attempt to promote the cross-linking reaction between humins and TGPh, 2,4,6-tris(dimethylaminomethyl)phenol was added to the mixture as the curing accelerator.

## EXPERIMENTAL SECTION

**Materials.** Triglycidyl ether of phloroglucinol with a repeating unit number ( $n$ ) between 0.5 and 1.2 was provided by Specific Polymers (Castriels, France). BDMA and the accelerator were purchased from Sigma-Aldrich (St. Louis, Missouri). Humins were provided by Avantium Chemicals as produced at the Avantium pilot plant in Geleen (Netherlands).

**Sample Preparation.** Humins were transferred into glass vials, weighed, and heated at 50 °C to reduce their viscosity. Then, BDMA (5% w/w) or the accelerator (5% w/w) or both (2.5% w/w each) were added and the mixture was vigorously mixed with a spatula and cured by increasing the temperature. When the copolymerization with TGPh (40% w/w) was performed, TGPh was added first to heated humins and another heating step at 50 °C was accomplished before the addition of BDMA and/or the catalyst (same percentages as for humins). After vigorous mixing, the samples were cured.

**Differential Scanning Calorimetry (DSC) Studies.** DSC measurements were conducted on a Mettler Toledo DSC 3 apparatus employing STARe software developed by Mettler Toledo. The instrument heat flow and temperature were calibrated in three points using water, indium, and zinc standards. Humins (55%), TGPh (40%), and the catalyst (BDMA 5%, accelerator 5%, and both 2.5% each) mixtures (10–12 mg) were directly put in 100  $\mu$ L aluminum DSC crucibles and heated. A temperature ramp of 10 °C/min was used under air (100 mL/min) over a temperature range of 25–250 °C.

**In Situ ATR-FTIR Analysis.** FTIR analysis was performed with a Nicolet iS50 FTIR spectrometer using attenuated total reflection mode with GladiATR equipment from PIKE Technologies. The spectra were

## Scheme 1. Schematic Representation of Epoxide Polymerization Catalyzed by a Tertiary Amine

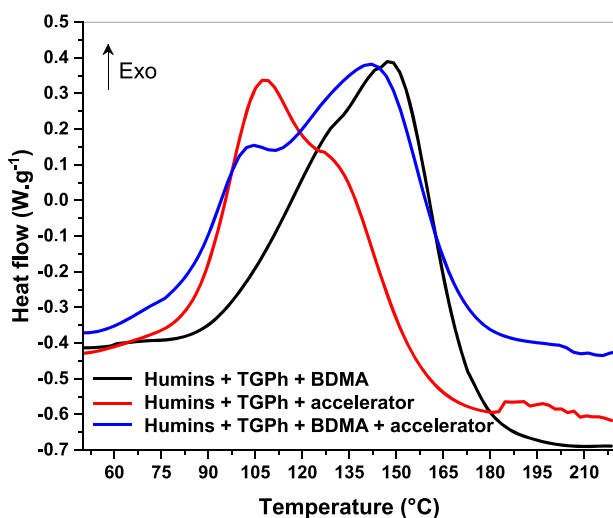
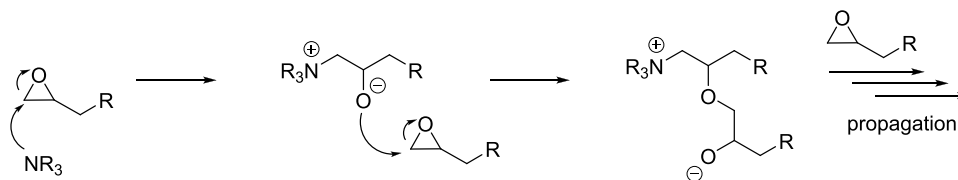


**Figure 3.** Comparison between humin and TGPh copolymerization reactions in the presence of BDMA (black line), the accelerator (red line), and BDMA + accelerator (blue line) by dynamic DSC at 10 °C/min.

recorded between 4000 and 600  $\text{cm}^{-1}$ , with 32 scans and a resolution of 4  $\text{cm}^{-1}$ . Automatic background subtraction was applied. The spectra of BDMA, the accelerator, humins, and TGPh were recorded at 30 °C. Humins were heated at 50 °C until the viscosity decreased and were mixed with 5% w/w BDMA and 5% w/w accelerator, separately, and with the mixture of both (2.5% w/w each). The samples were then heated on the ATR crystal from 30 to 150 °C with a temperature ramp of 10 °C/min. The same procedure was followed for TGPh and for humin–TGPh (55–40% w/w) mixtures. The spectra of humins were normalized with respect to the peak at 1667  $\text{cm}^{-1}$ , and the spectra of TGPh and the mixture were normalized with respect to TGPh aromatic C=C (the peak at 1592  $\text{cm}^{-1}$ ).

**NMR Analysis.** To perform NMR analysis, humins (55% w/w) and TGPh (40% w/w) were heated to decrease the viscosity and were mixed with BDMA (5% w/w), the accelerator (5% w/w), or both (2.5% w/w each). The samples were heated at 60, 70, 80, and 90 °C for 15 min, collecting a sample to record NMR spectra at each temperature point. The samples were dissolved in dimethyl sulfoxide ( $\text{DMSO}-d_6$ ); for the mixture of both BDMA and the accelerator, the sample heated at 90 °C was not soluble. An Ultra Shield Bruker spectrometer operating at 400 MHz  $^1\text{H}$  (100 MHz  $^{13}\text{C}$ ) was used to record the spectra.

Monodimensional  $^1\text{H}$ ,  $^{13}\text{C}$ , and distortionless enhancement by polarization transfer (DEPT)135 experiments were carried out with 16, 1024, and 256 scans and on spectral widths of 20, 238, and 160 ppm, respectively. Two-dimensional (2D) multiplicity-edited  $^1\text{H}$ – $^{13}\text{C}$  heteronuclear single quantum coherence (HSQC) and  $^1\text{H}$ – $^{13}\text{C}$  heteronuclear multiple bond correlation (HMBC) experiments were carried out with 2048 and 1024 data points over 13 and 9.5 ppm spectral widths, respectively, in F2 dimension using four scans and with 256 data points and 165 and 220 ppm spectral widths, respectively, in F1 dimension. The blank spectra of humins, TGPh, BDMA, and the accelerator were recorded as well. The spectra processing was accomplished with Topspin 4.0. The central DMSO solvent peak was used as the internal chemical shift reference ( $\delta_{\text{H}} = 2.50$  ppm,  $\delta_{\text{C}} = 39.5$  ppm), and as the intensity reference for the proton spectra, the aromatic peak of TGPh ( $\delta_{\text{H}} = 6.35$  ppm) was used. The spectra were phase-corrected, aligned, and integrated with MestReNova software.

## RESULTS AND DISCUSSION

**DSC Preliminary Studies.** DSC investigations were conducted to study the thermally induced copolymerization between humins and TGPh. Figure 3 shows the DSC curves comparing the reactivity as a function of the used catalyst. Each

**Table 1.** Humin FTIR Spectrum Assignments

wavenumber ( $\text{cm}^{-1}$ )	assignment
3350	$\nu(\text{OH})$
3117	$\nu(\text{CH sp}^2)$
2930, 2837	$\nu(\text{CH sp}^3)$
1708	$\nu(\text{C}=\text{O})$ aliphatic acids, esters, and saturated ketones
1667	$\nu(\text{C}=\text{O})$ aldehydes; conjugated ketones, i.e., $\beta$ -diketones, $\alpha\beta$ -unsaturated ketones, and aromatic ketones; conjugated acids; $\gamma$ -keto acids/esters
1612, 1517	$\nu(\text{C}=\text{C})$ conjugated with aromatics, double bonds, and carbonyls
1449, 1398	$\nu(\text{C}=\text{C})$ furan rings
1362	$\nu(\text{CO}-\text{OC})$ esters
1277, 1190	$\nu(\text{CO})$ ethers, hemiacetals, acetals, and furans
1073	$\nu(\text{CO})$ esters ( $\text{COO}-\text{C}$ ), ethers, hemiacetals, acetals, and furans
1019	$\nu(\text{CO})$ hydroxymethyl group
966, 946	$\delta(\text{C}-\text{C}-\text{C})$ and $\nu(\text{CO})$ of differently substituted furan rings
805, 768	$\pi(\text{CH})$ of differently substituted furan rings

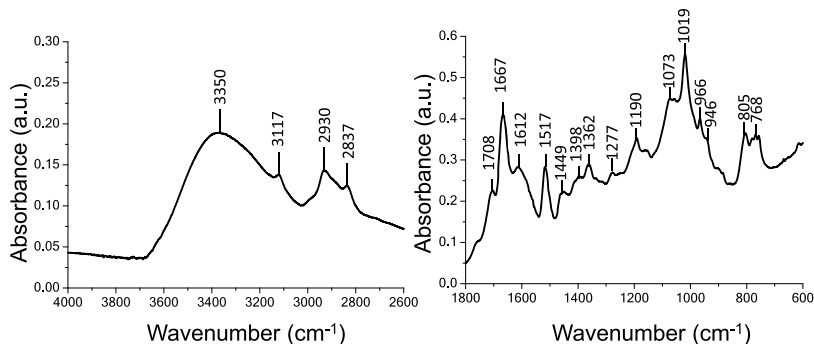


**Figure 4.** FTIR spectrum of humins.

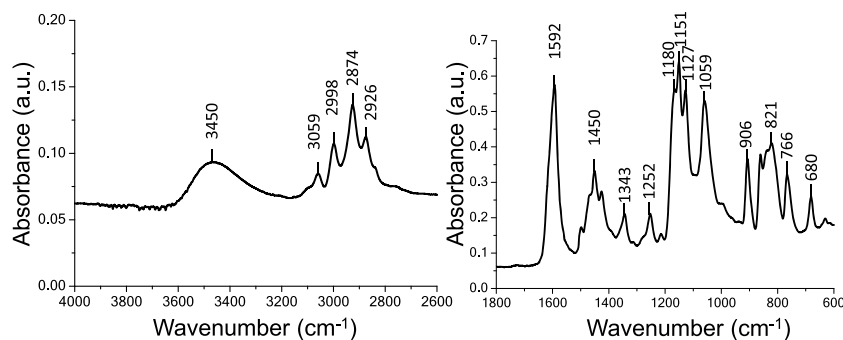
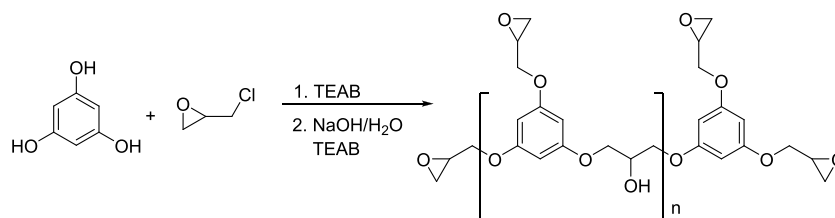


Figure 5. FTIR spectrum of TGPh.

### Scheme 2. TGPh Synthesis with Epichlorohydrin<sup>39,a</sup>



<sup>a</sup>TEAB stands for benzyltriethyl ammonium chloride

humins–TGPh formulation contains a ratio of 5% by the weight of the catalyst: BDMA, the accelerator, and (BDMA + accelerator). In the presence of the accelerator as the catalyst, a complex reactivity was observed since two exothermic peaks can be distinguished in the dynamic DSC curve, one major at a lower temperature of around 100 °C and a second one at 125 °C approximately. The shape of the curve suggests that the reaction is fast, with the heat flow curve rising very fast with an abrupt slope. In the case of BDMA, the reaction starts at a higher temperature compared with the accelerator, with the reaction being less rapid this time. Finally, the combination of the two catalysts produces a reaction that is the additional contribution of the individual catalyst to the humins–TGPh reactivity, with both BDMA and accelerator system reaction peaks being identified in this formulation.

**ATR-FTIR Spectroscopy. Characterization of Humins and Triglycidyl Ether of Phloroglucinol.** The IR spectrum of humins (Figure 4) shows the typical features reported before.<sup>5–7</sup> The main functional groups that can be found are the hydroxyl group involved in hydrogen bonds (the broad peak at 3350 cm<sup>-1</sup>), the carbonyl group belonging to aldehydes, ketones, acids, and esters (1708 and 1667 cm<sup>-1</sup>), the aromatic furan ring (several signals between 1667 and 768 cm<sup>-1</sup>), and the carbinol (from 1362 to 1019 cm<sup>-1</sup>). The presence of both sp<sup>2</sup> C–H and sp<sup>3</sup> C–H is evidenced by the peaks before and after 3000 cm<sup>-1</sup> (3117, 2930, and 2837 cm<sup>-1</sup>), respectively. More detailed assignments are reported in Table 1.

The triglycidyl ether of the phloroglucinol IR spectrum is reported in Figure 5. The stretching of aromatic CH gives rise to a peak at 3059 cm<sup>-1</sup>; aliphatic CH is instead responsible for the peaks at 2998, 2926, and 2874 cm<sup>-1</sup>. The strong peak at 1592 cm<sup>-1</sup> corresponds to aromatic C=C bonds, and the one at 1450 cm<sup>-1</sup> reflects the alkane CH bending. From 1214 to 1059 cm<sup>-1</sup> are located the bands of CO stretching (epoxides, ethers, and alcohols). In the last part of the spectrum, the most important peaks are those at 906 and 760 cm<sup>-1</sup>, which refer to C–C stretching and bending of the epoxy moieties, respectively.

At 3450 cm<sup>-1</sup>, a broad peak can clearly be seen. This band corresponds to the hydroxyl functionality whose bending peaks are at 1343 and 1252 cm<sup>-1</sup>. The presence of –OH groups comes from epoxide ring opening that is reported to occur during phloroglucinol glycidylation, as described in Scheme 2.<sup>38,39</sup> All of the assignments are reported in Table 2.

Table 2. TGPh FTIR Spectrum Assignment

wavenumber (cm <sup>-1</sup> )	assignment
3450	$\nu(\text{OH})$
3059	$\nu(\text{CH sp}^2)$
2998, 2926, 2874	$\nu(\text{CH sp}^3)$
1592	$\nu(\text{C}=\text{C})$
1450	$\delta(\text{CH sp}^3)$
1343, 1252	$\delta(\text{OH})$
1180	$\nu(\text{CO})$ epoxides
1151, 1127	$\nu(\text{CO})$ ethers
1059	$\nu(\text{CO})$ alcohols
906, 766	$\nu(\text{CC})$ and $\delta(\text{CC})$ epoxide
821	$\delta(\text{C}=\text{C})$
680	$\pi(\text{CH})$

**Auto-Cross-Linking of Humins and Triglycidyl Ether of Phloroglucinol.** To evaluate the onset of auto-cross-linking of humins and triglycidyl ether of phloroglucinol, the two macromonomers were tested separately with BDMA and the accelerator at increasing temperatures (30–150 °C). The in situ FTIR experiments of humins in the presence of BDMA, the accelerator, and both (Figure 6) show a progressive narrowing and shift toward higher wavenumbers of the band at 3350 cm<sup>-1</sup>, indicating a reduced extent of hydrogen bonds for the hydroxyl groups. In addition, a decrease in the band intensity was observed. It should be noted that the presence of the accelerator, which bears itself a hydroxyl group, broadens a lot the band in the first points of the temperature ramp because of the intermolecular hydrogen bonding between the accelerator and the humins. Furthermore, signals coming from BDMA and the

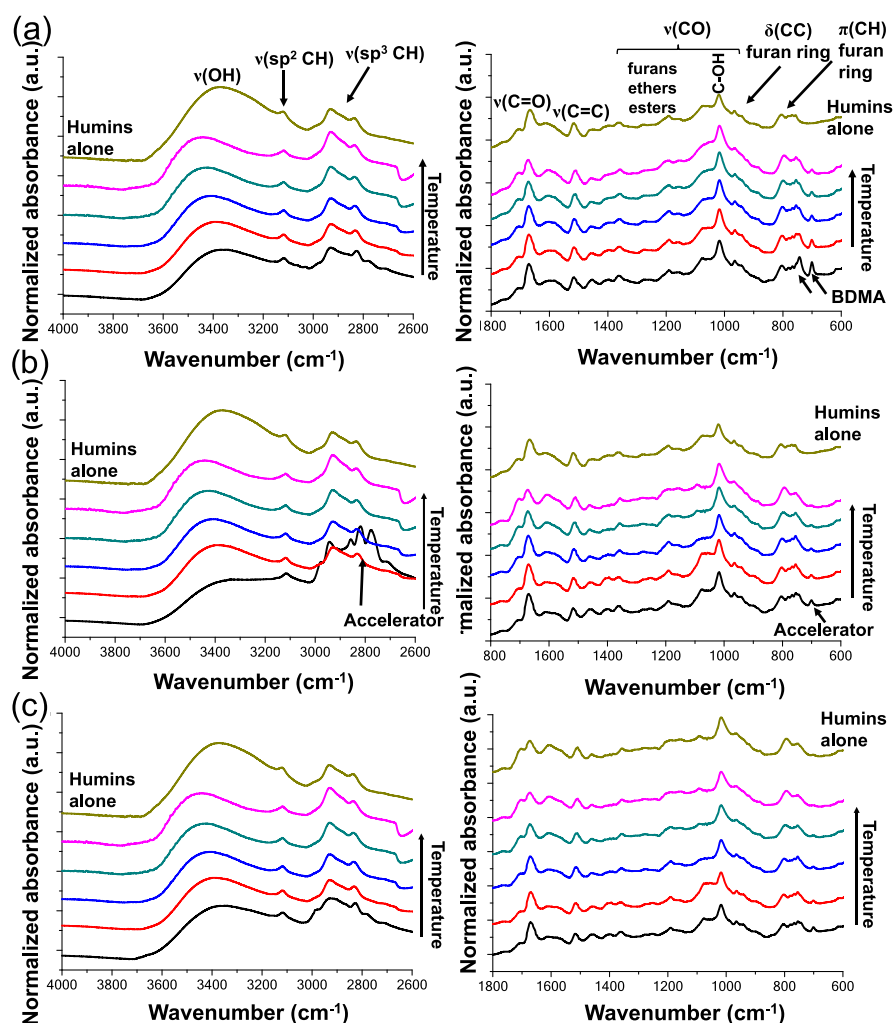


**Figure 6.** IR spectra of humins with (a) BDMA, (b) accelerator, and (c) both at increasing temperatures: 30 °C in black, 60 °C in red, 90 °C in blue, 120 °C in green, and 150 °C in magenta. The blank spectrum of humins is colored in ochre, and in the first panel, the assignment is reported. The arrows indicate the signals from BDMA or from the accelerator.

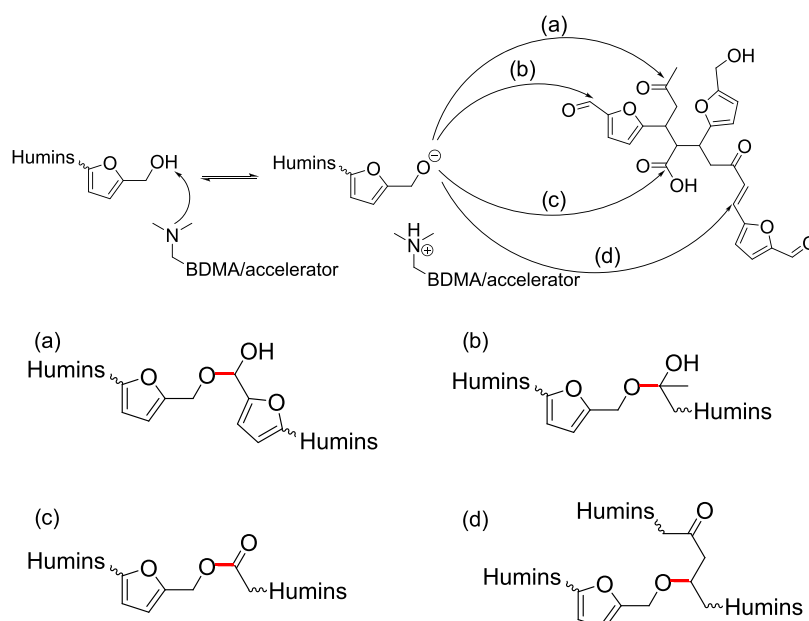
accelerator were observed in different parts of the spectrum (indicated by arrows in the figures) but only in the first temperature reaction range. Peaks coming from  $sp^2$  and  $sp^3$  C–H bonds of humins remain constant. In general, the last part of the spectra (from 1500 to 600  $cm^{-1}$ , approximately) becomes much broader. The peaks that correspond to carbonyls and to conjugated double bonds increase their intensity upon raising the temperature. The CH wagging of the furan ring proved to be perturbed by the presence of both BDMA and the accelerator. Particularly, the furan peak at 805  $cm^{-1}$  undergoes a shift toward lower frequencies. Spectral changes appear with a different extent and at different temperatures considering the presence of BDMA, the accelerator, and both. The combination of BDMA and the accelerator proved to affect more the molecular structure of humins. All of these features suggest a rearrangement of the furanic structure involving mainly the carbonyl functional groups. The hardening of the material, furthermore, worsens the contact between the material and the ATR crystal, leading to considerable IR spectrum broadening.

Possible routes to the structural rearrangement of humins can be due to auto-cross-linking by condensation through the nucleophilic attack and/or by additional aromatization. However, the addition of the hydroxyl to ketones and aldehydes would lead to a carbonyl content decrease and does not explain the hydroxyl

decrease because the hydroxyl that is consumed is replaced by the OH of the hemiacetal product (Scheme 3a,b). However, hemiacetals are unstable species that can easily undergo decomposition into the carbonyl and the alcohol under basic conditions. Deprotonation of the hydroxyl by the tertiary amine starts the mechanism, and the resulting anionic oxygen can dismiss an alkoxide as a leaving group to give the carbonyl compound. Last, the alkoxide is converted into a hydroxyl by the protonated tertiary amine (Scheme 4). The formation of acetals under basic conditions is not possible because to add another alkoxide, the hydroxyl must be removed, and if not protonated,  $-OH$  is a bad leaving group. The alcoholic function can moreover be responsible for the esterification of carboxylic acids (Scheme 3c), but in this scenario, the carbonyl function is preserved. The hydroxyl group can also add to  $\alpha,\beta$ -unsaturated ketones. Usually, the addition takes place at the  $\beta$  carbon, leading to the formation of a new ether bond (Scheme 3d). This reaction would lead to a decrease in the hydroxyl content, but it also implies a decrease in the conjugation that was not observed and does not explain the change in the carbonyl bands.

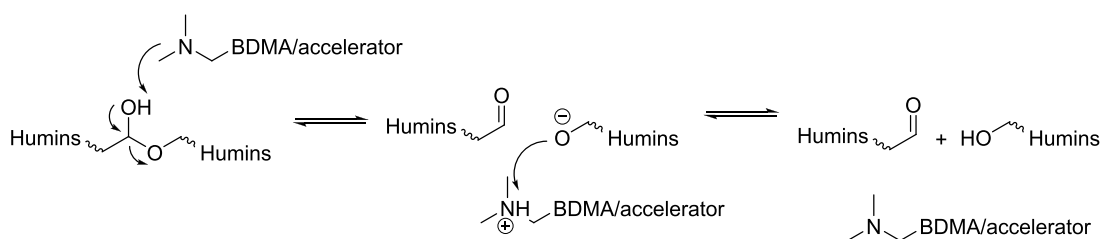
Polyaromatization, beyond leading to additional changes in the spectra that were not found, was reported to start only from 170 °C<sup>7</sup> or to be acid-catalyzed.<sup>5</sup> Hydrolytic rupture of the furan ring could explain the increase in the carbonyl content, but it

**Scheme 3. Nucleophilic Attack of the Deprotonated Hydroxyl of Humins to the Carbonylic and  $\alpha\beta$ -Unsaturated Carbonylic Functions of Humins<sup>a</sup>**



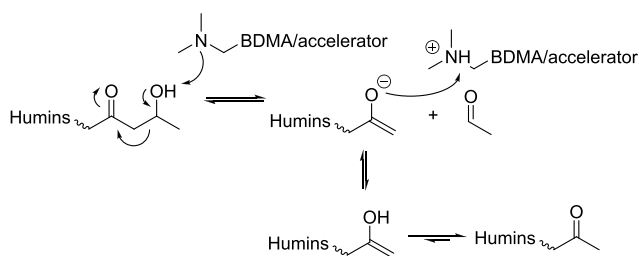
<sup>a</sup>The possible products are (a, b) hemiacetals, (c) esters, and (d) ethers. The new bonds are colored in red.

**Scheme 4. Hemiacetal Decomposition**



occurs only under strong acidic conditions.<sup>5</sup> The increase in the carbonyl content and the decrease in the hydroxyl one can be related to a retro-aldol reaction, which was reported to be a common route in carbohydrate and biomass degradation.<sup>3,40</sup> Actually,  $\beta$ -hydroxy ketone retro-aldol reactions were found to contribute to sugar-degradation pathways at high temperature and under basic catalysis.<sup>41,42</sup> The mechanism is started by the hydroxyl deprotonation by the tertiary amine and the rupture of the bond between  $\alpha$  and  $\beta$  carbons, giving a deprotonated enol and an aldehyde. After the enol protonation and its tautomerization, the ketone is formed (Scheme 5).

**Scheme 5.  $\beta$ -Hydroxy Ketone Retro-Aldol Reaction**



Another interesting reversible reaction that can take place is the  $\gamma$ -keto acid cyclization. The presence of  $\gamma$ -keto acid groups bound covalently to the humin structure has already been

reported by van Zandvoort et al.<sup>16</sup> The respective positions of these two functional groups allow mainly two different cyclization routes. In the first, the acid can be deprotonated by the tertiary amine and attack the electrophilic ketone carbonyl. Then, the protonated tertiary amine transfers a hydrogen to the alkoxide (Scheme 6a). In addition, the ketone in its enol form, after being deprotonated by the tertiary amine, can add to the carbonyl of the acid, leading to a  $\beta,\gamma$ -unsaturated lactone that can tautomerize in an  $\alpha,\beta$ -unsaturated lactone (Scheme 6b). These pathways can explain the increase in the conjugation system, but they involve a decrease in the carbonyl content.

There is not a unique mechanism that can explain all of the IR spectral modifications but, considering the abundance of reactive functional groups in humins, different reaction mechanisms are expected to take place at different extents depending on the conditions inducing complex molecular changes.

Concerning TGPh, when it was mixed with BDMA, the accelerator, or both, as the temperature increases, the OH band rises and broadens and a new band appears at a lower frequency, indicating intramolecular hydrogen bonding. Furthermore, the linear  $sp^3$  CH, the ether, and the alcoholic CO peaks increase in intensity. Meanwhile, the intensities of epoxide CO and the two epoxy CC peaks are reduced (Figure 7). All of these features are consistent with epoxide ring opening and additional homopolymerization. As can be seen in Figure 8, the spectra of BDMA and the accelerator could not be responsible for the changes observed.

Scheme 6. Possible Routes of the Cyclization of  $\gamma$ -Keto Acids: (a) Intramolecular Nucleophilic Attack and (b) Intramolecular Esterification

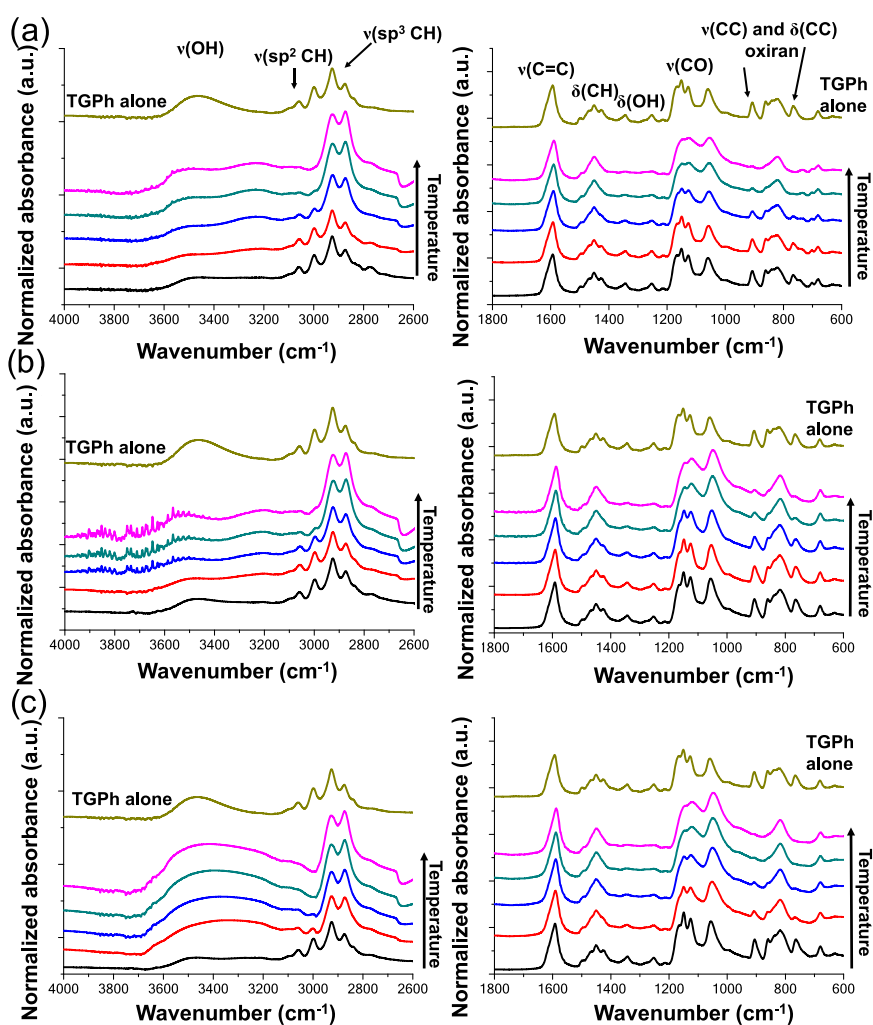
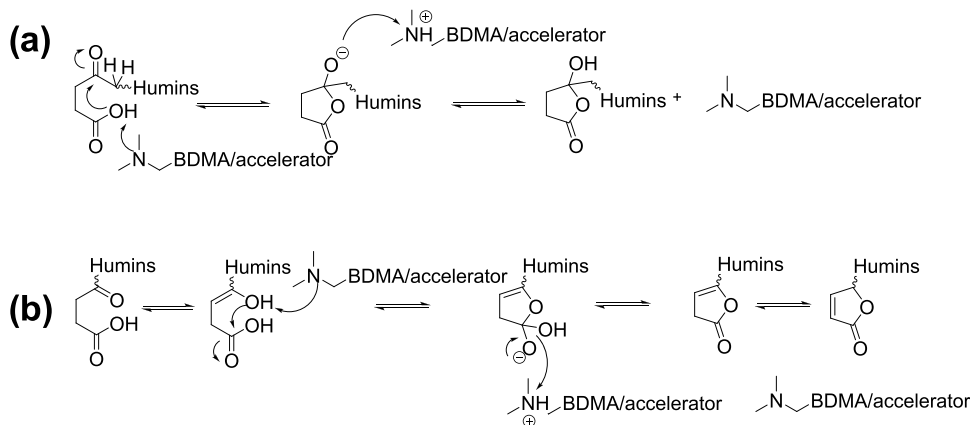
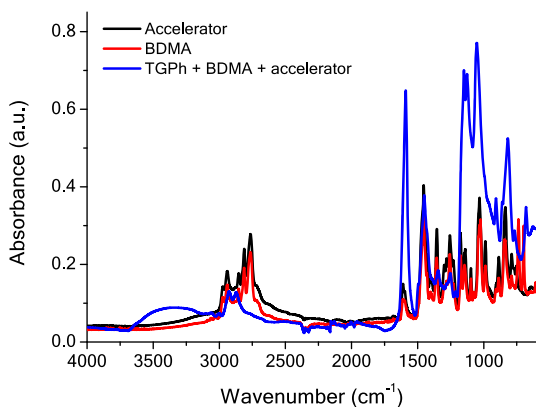


Figure 7. IR spectra of TGPh with (a) BDMA, (b) accelerator, and (c) both at increasing temperatures: 30 °C in black, 60 °C in red, 90 °C in blue, 120 °C in green, and 150 °C in magenta. The TGPh blank spectrum is colored in ochre.

The reaction is initiated by the nucleophilic attack of the tertiary amine at the epoxy group followed by a proton transfer from the TGPh hydroxyl function to the opened epoxy ring. Then, the alkoxide group reacts with another epoxide and the adduct formed again exchanges one proton with another hydroxyl group, propagating the polymerization. The tertiary amine can be regenerated by the nucleophilic exchange with the alkoxide (Scheme 7).

The combination of both BDMA and the accelerator induced the auto-cross-linking reaction to a higher extent as can be inferred from the much larger effects on the IR spectra (Figure 7c), suggesting a reactivity increase due to the accelerator presence.

*Copolymerization of Humins and Triglycidyl Ether of Phloroglucinol.* When humins and TGPh are reacted in the presence of BDMA (Figure 9a) or the accelerator (Figure 9b),



**Figure 8.** Overlapped FTIR spectra recorded at 30 °C of the accelerator (black), BDMA (red), and the mixture of TGPh, BDMA, and the accelerator at 60 °C (blue).

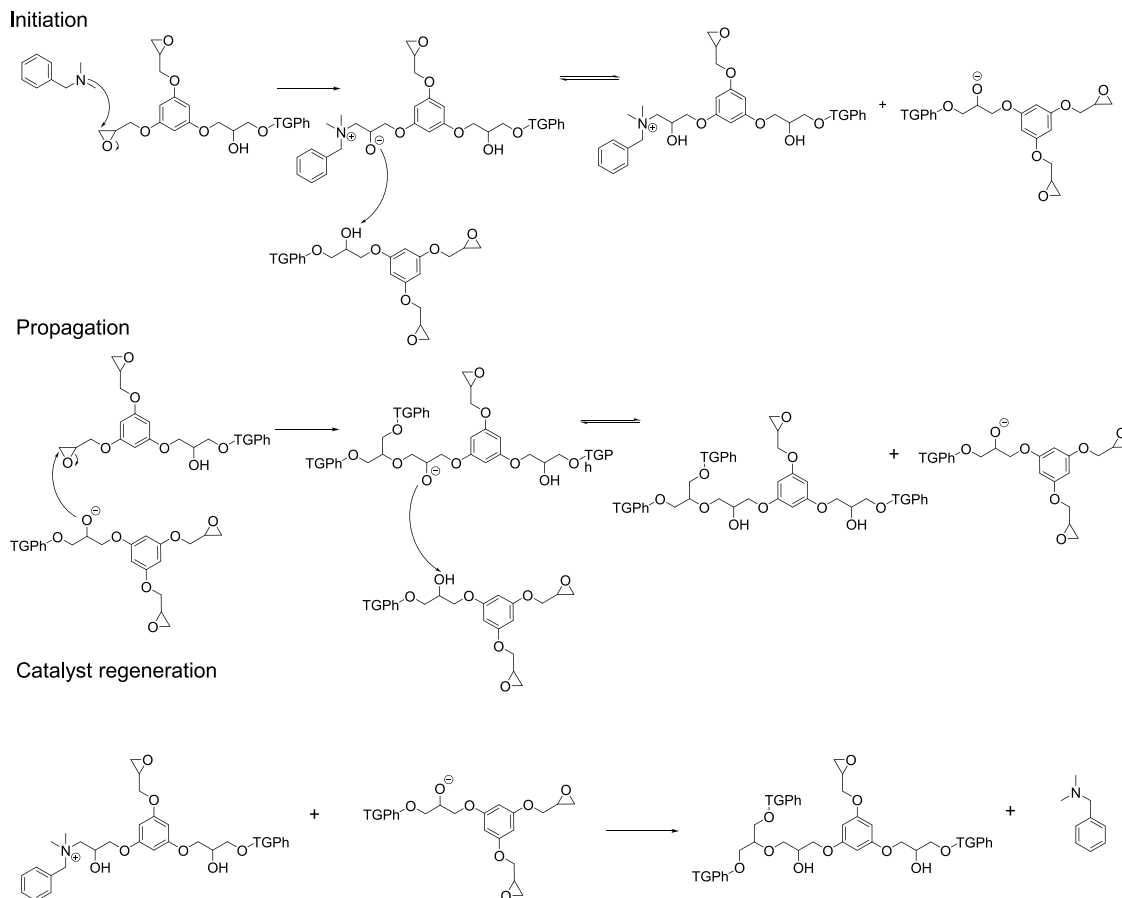
the hydroxyl band remains quite constant in the first points of the temperature ramp and then slightly increases. The linear  $\text{sp}^3$  CH signals increase as the temperature rises. In the spectrum with BDMA, there is a problem in the background subtraction, but the intensity increase of the peaks below  $3000\text{ cm}^{-1}$  can still be ascertained. Again, the spectrum region going from  $1800$  to  $600\text{ cm}^{-1}$  is affected by a remarkable broadening of the bands. The humin carbonyl at  $1708\text{ cm}^{-1}$  and the conjugated carbon double bond peaks present a very low intensity from the beginning, which remains rather constant. The humin C=O peak at  $1667\text{ cm}^{-1}$  decreases while increasing the temperature until it

vanishes. An increase in the intensity is observed for the CO region; on the contrary, the TGPh epoxy carbon–carbon bond peaks progressively decrease. As for humins alone, there is a red shift at  $805\text{ cm}^{-1}$ .

The most evident difference when both BDMA and the accelerator are present (Figure 9c) is the increase of humin carbonyl (the C=O signal at  $1667\text{ cm}^{-1}$  after increasing slightly decreases at  $150\text{ °C}$ ) and conjugated C=C peaks. The other regions of the spectra show the same changes as with BDMA and the accelerator alone. The variations in TGPh signals indicate the opening of the epoxy functionalities. Humin signals change in a different way with respect to humins alone when BDMA and the accelerator are separately mixed with the two polymers; instead, when they are both in the mixture, the changes are similar to those observed for humins. To better clarify the molecular features that are responsible for these spectral changes, NMR analysis was performed.

**NMR Spectroscopy. Characterization of Humins and Triglycidyl Ether of Phloroglucinol.** The complex structure of humins is reflected in the challenging assignment of the NMR spectra. Few assignments were reported and usually refer to laboratory-prepared humins using  $^{13}\text{C}$  solid-state NMR aimed at identifying the linkages between furan rings.<sup>16,27</sup> In the proton spectrum (Figure 10a), it is possible to distinguish clearly some distinctive moieties of humins: the aldehydes (singlets at 9.57 and 9.54 ppm), the aromatic protons of furan rings (doublets at 7.50, 7.48, 6.75, 6.72, and 6.60 ppm), and the protons attached to carbons directly bound to furans (singlets at 4.62, 4.50, and 4.46 ppm). The region going approximately from 4 to 3 ppm is

#### Scheme 7. Proposed TGPh Homopolymerization Mechanism in the Presence of BDMA



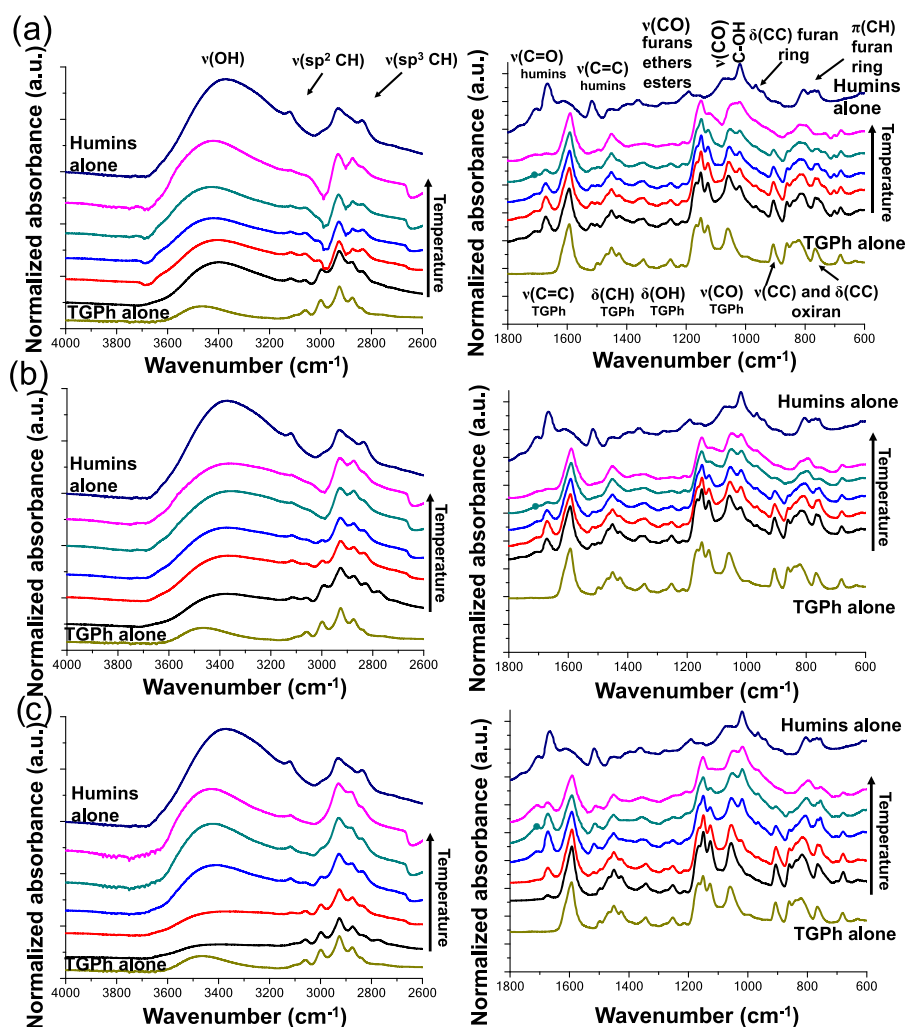


**Figure 9.** IR spectra of TGPh and humins with (a) BDMA, (b) accelerator, and (c) both at increasing temperatures: 30 °C in black, 60 °C in red, 90 °C in blue, 120 °C in green, and 150 °C in magenta. The TGPh blank spectrum is colored in ochre. The humin blank spectrum is colored in navy blue.

very dense and numerous peaks overlap. This region can be assigned to the protons bound to oxygenated carbons (ethers, hemiacetals, acetals, and hydroxyls). The more upfield peaks correspond to  $\alpha$  carbonyl protons, methine, methylene, and methyl groups. Considering the limited signal intensity of the 5–6.5 ppm region, it should be concluded that the presence of nonaromatic double bonds is negligible. The  $^{13}\text{C}$  spectrum (Figure 10b) confirms the presence of carbonyls (aldehydes and ketones at around 200 ppm and acids/esters at 180–160 ppm, approximately). Furan carbons are assigned as follows: from 150 to 165 ppm substituted  $C_{\omega}$ , from 135 to 150 ppm protonated  $C_{\omega}$ , from 125 to 135 ppm substituted  $C_{\beta}$ , and from 110 to 125 ppm protonated  $C_{\beta}$ . This assignment was based on published data<sup>16</sup> and was also confirmed by the DEPT135 spectrum (Figure 10c). The absence of peaks between 140 and 150 ppm suggests that protonated  $C_{\alpha}$  is not present, and the low intensity of substituted  $C_{\beta}$  peaks indicates the scarce abundance of furan linkages through  $C_{\beta}$ . Carbons directly bound to furans can be found between 70 and 50 ppm. The region going from 100 to 50 is very crowded, indicating a huge amount of alcohols, ethers, hemiacetals, and/or acetals, as opposed to previous findings.<sup>16</sup> This discrepancy is due to the different origin of the humins. The more shielded signals are related to  $\alpha$  carbonyl positions and to methine, methylene, and methyl groups of the carbonaceous

skeleton of the macromolecule. Some more information can be gained from 2D spectra. The multiplicity-edited  $^1\text{H}$ – $^{13}\text{C}$  HSQC spectrum shows the correlations between protons and carbons directly bound ( $^1J$ ), generating opposite signs between peaks of  $\text{CH}_2$  (negative) and  $\text{CH}/\text{CH}_3$  (positive). In the humin HSQC spectrum, most of the protonated carbons belong to  $-\text{CH}-$  groups and the main  $-\text{CH}_2-$  groups are those bound directly to the furan rings (Figure S1). These findings are in agreement with the previously proposed humin structure.<sup>16,23</sup>

Along with the HSQC spectrum, the  $^1\text{H}$ – $^{13}\text{C}$  HMBC spectrum was also recorded to assess the long-range C–H couplings ( $^2J$  and  $^3J$ ). The aldehydic protons show a correlation with the  $\alpha$  carbons of furan rings ( $\delta_{\text{H}} = 9.5$ ;  $\delta_{\text{C}} = 155$  ppm) (Figure 11a). Since no other correlations of aldehydic protons can be found in the HMBC spectrum, other connections can be ruled out. This finding is in agreement with the humin structure proposed by Baccile et al.<sup>23</sup> but not with the one proposed by van Zandvoort et al.<sup>16</sup> The splitting of the aldehydic signal in more than one peak should reflect different surrounding chemical environments inside the polymeric structure rather than a different bonding pattern. Starting from this correlation, it is possible to assign all of the terminal aldehydic furan fragments, as described in Figure 11a (black traces). Furanic  $\alpha$  carbons resonate at 163 and 152 ppm,  $\beta$  carbons at 124 and 110 ppm, and  $\beta$  protons at

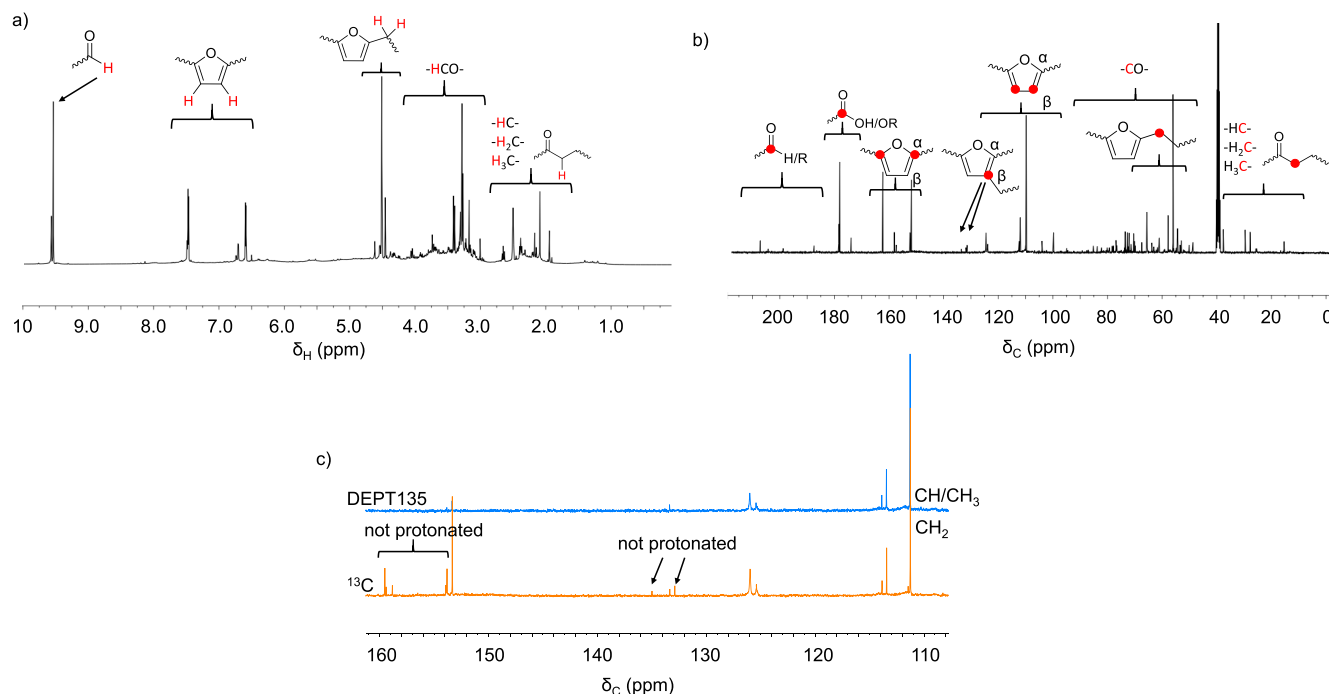


**Figure 10.** (a)  $^1\text{H}$ , (b)  $^{13}\text{C}$ , and (c) overlapped DEPT135 (blue) and  $^{13}\text{C}$  (orange) NMR spectra of humins. The proton and carbon assignments are depicted in red on humin structural fragments.

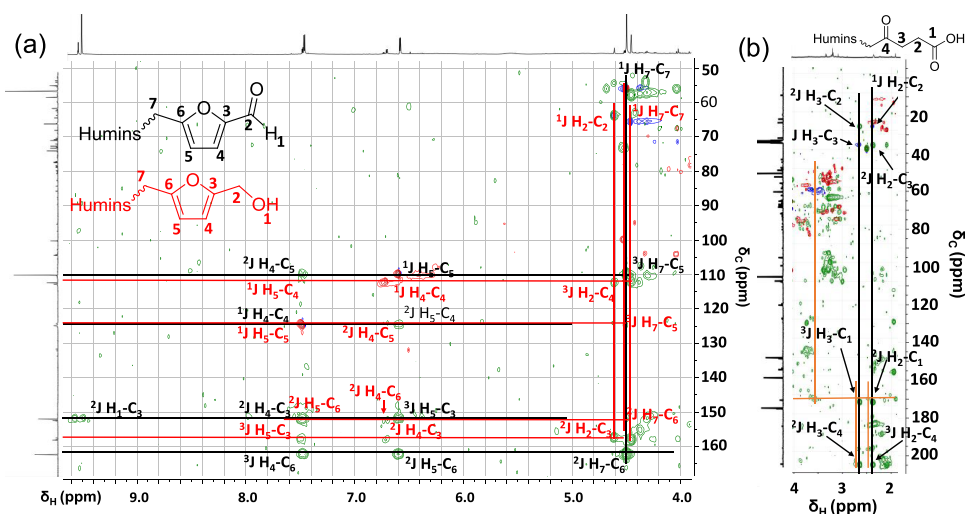


**Figure 11.** Enlargements of (a) furan and (b) carbonyl regions of superimposed multiplicity-edited  $^1\text{H}$ – $^{13}\text{C}$  HSQC spectrum (positive peaks in red and negative in blue) and  $^1\text{H}$ – $^{13}\text{C}$  HMBC spectrum (green) of humins. The whole spectra are given in Figure S1.

7.48 and 6.60 ppm. The methylene bound to the furanic carbon at the opposite side from the aldehydic function is represented by the peaks at 4.50 and 56 ppm for proton and carbon, respectively. Moreover, also the furanic structure whose  $\beta$  protons fall at 7.5 and 6.7 ppm was completely assigned (Figure 11a, red traces).

Furanic  $\alpha$  carbons and  $\beta$  carbons are at 158, 152 and 124, 112 ppm, respectively.  $\beta$  protons are at 7.50 and 6.72 ppm. There are two methylene groups bound to the furanic ring: one at  $\delta_{\text{H}} = 4.62$  and  $\delta_{\text{C}} = 64$  ppm and one at  $\delta_{\text{H}} = 4.46$  and  $\delta_{\text{C}} = 65.6$  ppm. It is likely that this structure corresponds to the terminal hydroxy methylene furan ring whose methylene protons are shifted downfield with respect to the others (4.62 ppm). As previously observed, the carbonyl groups appear to be located far from the furan rings, since they show correlations only with

the aliphatic protons. The carbon peak at 207.3 ppm shows no couplings with protons in the HSQC spectrum; therefore, it belongs to a ketone rather than to an aldehyde. In the HMBC spectrum, the correlation between the ketonic carbonyl at 207.3 ppm and the acidic carbonyl at 173.8 ppm with two methylene groups ( $\delta_{\text{H}} = 2.65/\delta_{\text{C}} = 37.6$  ppm and  $\delta_{\text{H}} = 2.38/\delta_{\text{C}} = 27.7$  ppm), which in turn are correlated with each other (Figure 11b, black traces), proves the occurrence of the  $\gamma$ -keto acid system. Another  $\gamma$ -keto acid system is present in a lower amount at slightly different frequencies (carbonyls at 207.1 and 172.3 ppm and methylene protons at 2.70 and 2.47 ppm), indicating a different chemical environment or the esterification of the acid (Figure 11b, orange lines). This last hypothesis appears to be confirmed by the presence of another correlation peak at 3.57 ppm ( $\delta_{\text{H}}$ ) at the same chemical shift of the carbonyl

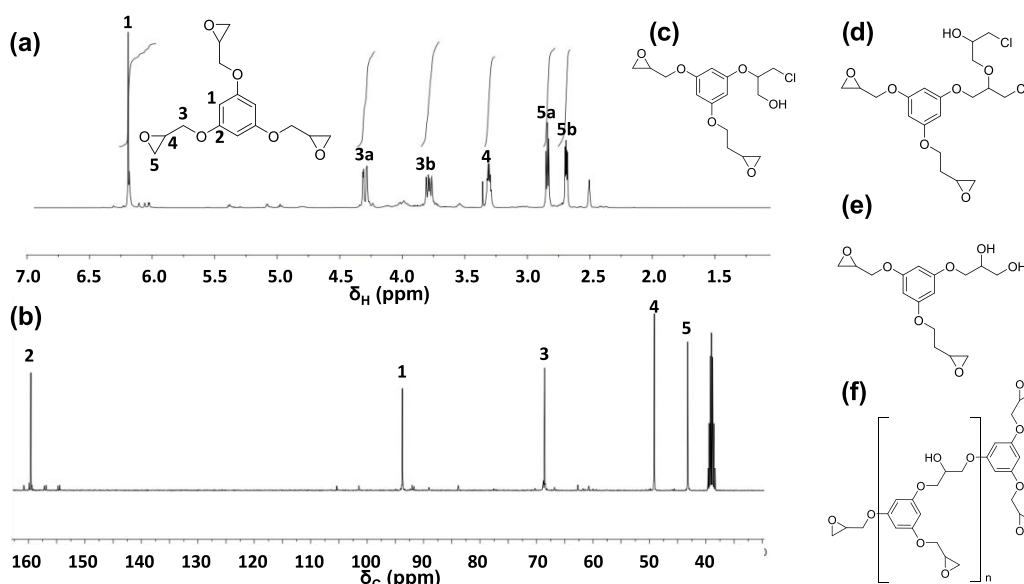


**Figure 12.** (a)  $^1\text{H}$  and (b)  $^{13}\text{C}$  NMR spectra of TGPh with the related assignments. The structures of glycidylation side-reaction products from (c) epichlorohydrin polyaddition, (d) formation of  $\beta$ -chlorohydrin, (e) formation of  $\alpha$ -glycol, and (f) homopolymerization are reported.

at 172.3 ppm ( $\delta_{\text{C}}$ ) (Figure 11b). Furthermore, this proton is directly bound to a carbon that resonates at 51.53 ppm. The proton (3.57 ppm) and the carbon (51.53 ppm) values are compatible with those of an ester. However, the nature of the alcohol that gives this ester could not be identified because no other significant correlations could be seen in the HMBC spectrum. In Figure 12, the assignment of the proton (a) and of the carbon (b) NMR spectra of TGPh is depicted. The proton assignment was based on data reported in the literature,<sup>39</sup> and the carbon assignment was confirmed by recorded 2D spectra (Figure S2). The two spectra highlighted the presence of products coming from phloroglucinol glycidylation side-reactions like epichlorohydrin polyaddition (Figure 12c), the formation of  $\beta$ -chlorohydrin (Figure 12d), the formation of  $\alpha$ -glycol (Figure 12e), and homopolymerization (Figure 12f).

**Copolymerization of Humins and Triglycidyl Ether of Phloroglucinol in the Presence of BDMA.** By comparing the  $^1\text{H}$  NMR spectra of humins, TGPh, BDMA, and the mixture of the three at 60 °C (Figure 13a), two new aromatic proton doublet signals at 7.59 and 7.52 ppm were observed, suggesting the formation of a new furanic species. Other doublet signals appear at 4.66, 3.50, and 3.07 ppm. The analysis of 2D spectra reveals that these new peaks are all correlated through carbon–proton couplings (Figure 13b), meaning that they belong to the same structure.

At the same time, the cross-peaks assigned to the hydroxymethyl terminal furan disappeared from the spectra, suggesting that the new species originates from it (Figure 13d). Furthermore, as the temperature increases, TGPh proton epoxide signals show a progressive intensity decrease (Figure 14a). These pieces of evidence point at the formation of cross-links between humins and TGPh through the nucleophilic opening of the TGPh oxirane ring by the hydroxyl function of humins (Figure 13c). This hypothesis is confirmed also by following the correlation system in the 2D spectra (Figure 13b). The two new aromatic peaks (H1 and H2) are coupled with a new methylene signal at 4.66 ppm (H4). The latter is coupled with the peak at 3.07 ppm (H5), which correlates with the peak at 3.50 (H6). Surprisingly, the attack of  $-\text{OH}$  does not involve the less

substituted epoxide carbon, as expected in an  $\text{S}_{\text{N}}2$  under basic conditions, but the hydroxy methylene proton revealed to be coupled with a  $-\text{CH}-$  group (positive in the HSQC spectrum). This atypical regioselectivity is likely to be related to the reciprocal position of humins and TGPh due to the establishment of  $\pi-\pi$  interactions between the aromatic rings of TGPh and the furan rings of humins. This interaction would orient the molecules in a way in which the more substituted carbon of the epoxide is closer to the hydroxyl that actually attacks it. The splitting of proton signals is related to their stereochemical relationship. The described opening of the oxirane ring leads to the formation of a new stereocenter in position 5. Considering the three-dimensional complexity of the cross-linked structure, steric hindrance prevents free rotation around C–C bonds.

The two enantiomers are therefore characterized by different chemical environments, and the enantiomeric protons in position 5 resonate at different chemical shifts (3.10 and 3.06 ppm). The protons in position 6 are diastereotopic, and they split into two signals as expected (3.53 and 3.46 ppm for proton and 63.6 and 66.4 ppm for carbon). The two protons in position 4 are enantiotopic, and since their rotation is forbidden, they are not equivalent, giving two different correlation signals at 4.69 and 4.61 ppm. This cross-linking scenario is further supported by the presence of new CH carbon signals in the DEPT 135 spectrum in the furanic region (Figure 15a).

The heteropolymerization is likely to proceed through an anionic polymerization (Scheme 8) in which the first step is the nucleophilic attack of BDMA to TGPh epoxide followed by a proton transfer between the new adduct and the hydroxyl of humins. The alkoxide of humins formed in this way opens an oxirane ring, creating a new bond between TGPh and humins. A series of proton exchanges propagate the polymerization reaction. BDMA is then regenerated by nucleophilic exchange with a humin alkoxide.

By comparing the HMBC spectra of humins alone and of humins mixed with TGPh and BDMA, a decrease in the intensity of carbonyl correlation peaks can be observed (Figure 15b), in agreement with IR results. However, the spectra do not present clear evidence of new bonds formed by nucleophilic

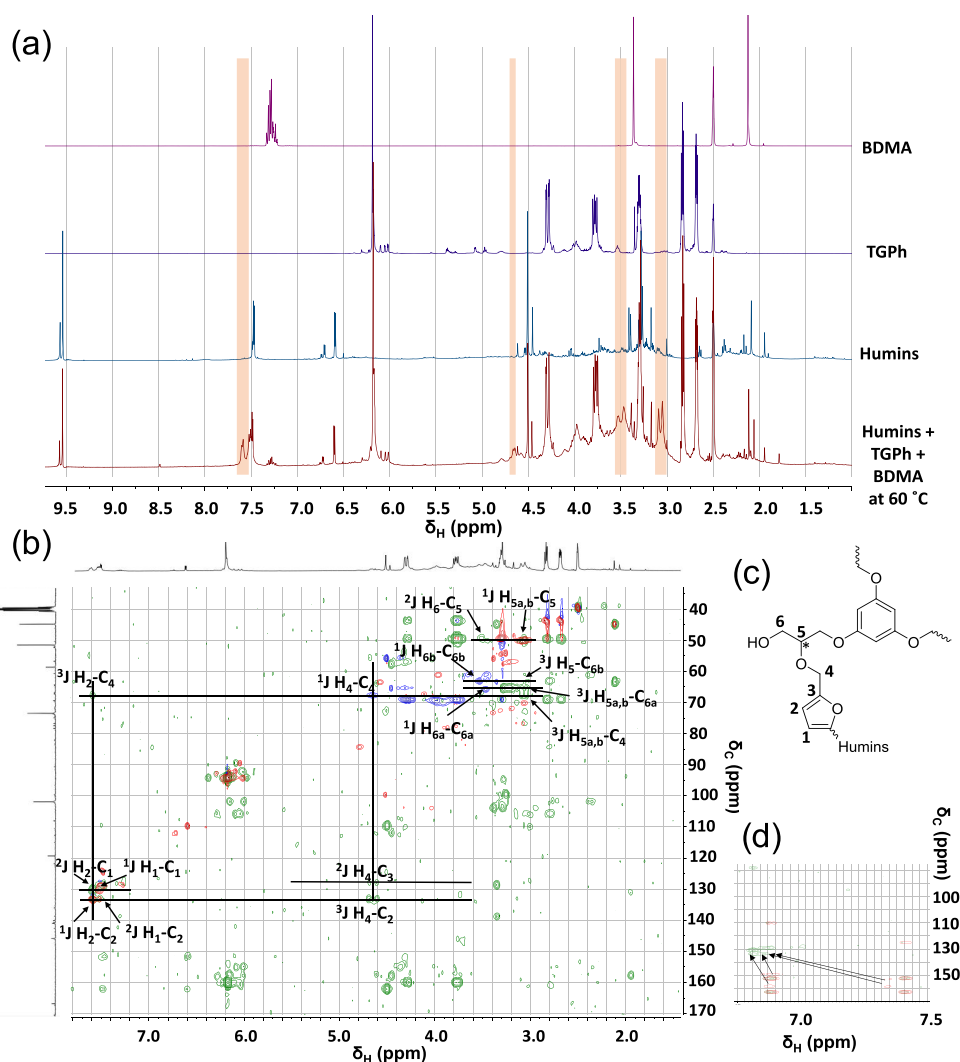


**Figure 13.** (a) Stacked  $^1\text{H}$  NMR spectra of BDMA (purple), TGPh (violet), humins (petrol), and the mixture of all at 60 °C (maroon). The new peaks appearing in the last sample are highlighted in orange. (b) The superimposition of the multiplicity-edited  $^1\text{H}$ - $^{13}\text{C}$  HSQC spectrum (positive peaks in red and negative in blue) and  $^1\text{H}$ - $^{13}\text{C}$  HMBC spectrum (green) of the humins, TGPh, and BDMA mixture at 60 °C. (c) Proposed cross-linking between humins and TGPh based on NMR data. (d) Overlapped  $^1\text{H}$ - $^{13}\text{C}$  HMBC spectra (furanic region) of the humins, TGPh, and BDMA mixture at 60 °C (green) and of humins alone (red) showing the appearance of the new furanic species and the disappearance of the hydroxy methylene furan system.

addition to carbonyls. Considering the aldehydes, the proton signal undergoes a little shift, but its intensity remains constant (Figure S3); therefore, the formation of hemiacetals can be ruled out. The  $\gamma$ -keto acid system presents a remarkable shift and an intensity decrease (Figure 15b). The shift can be correlated with an esterification of the acidic group by a hydroxyl function, but no new correlations can be found to prove this hypothesis (see Figure S4).  $\gamma$ -Keto acids can give cyclization, as already explained (Scheme 6). These reactions produce the partial conversion of carbonyl carbons to aliphatic ones and therefore they can explain the decrease in the carbonyl content. In addition, the carbonyls that are preserved, after the cyclization, experience a different chemical environment that can reflect the variation of the chemical shift. Other correlation peaks decrease their intensity, i.e., 3.74  $\delta_{\text{H}}$ /132.43  $\delta_{\text{C}}$  ppm, 3.74  $\delta_{\text{H}}$ /147.1  $\delta_{\text{C}}$  ppm, 3.71  $\delta_{\text{H}}$ /131.7  $\delta_{\text{C}}$  ppm, and 1.90  $\delta_{\text{H}}$ /172.6  $\delta_{\text{C}}$  ppm (Figure S4), but the lack of their unambiguous assignment does not allow inferring any related structural changes so far. The increased viscosity of the samples as the temperature increases affects the quality of the spectra, broadening the signals and leading to problems in the magnetic field homogeneity. However, some

features can still be observed. Increasing the temperature from 60 to 90 °C, the intensity of TGPh epoxy proton signals further decreases (Figure 14a). This intensity reduction was used to calculate the epoxy conversion percentage. To do this calculation, the intensity of protons in position 5 was used because they are less overlapped. At 60 °C, the conversion was approximately 30%, and at 90 °C, it reached 40% following a linear trend (Figure 14b,c). Furthermore, the rising temperature induces the complete disappearance of the  $\gamma$ -keto acid system (Figure 16). This is consistent with the  $\gamma$ -keto acid cyclization scenario, considering that this reaction is usually favored by an increase in temperature. On the contrary, a slight increase in the  $\gamma$ -keto ester system was observed (Figure 16). Probably, these two systems are related, and as the temperature increases, the esterification becomes more recurring. As observed with FTIR, BDMA signals disappear as the temperature increases (Figure 16). This is likely to be due to the trapping of the catalyst inside the growing viscous polymer matrix. This entails a lower tumbling rate of the molecule, which leads to a consistent broadening of the corresponding signals and thus a decreased intensity.

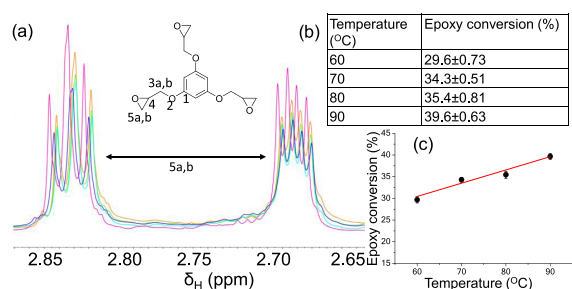


**Figure 14.** (a) Enlargement of  $^1\text{H}$  TGPh epoxy peaks at increasing temperatures: TGPh in pink; TGPh with humins and BDMA at 60 °C in orange, at 70 °C in green, at 80 °C in cyan, and at 90 °C in blue. The whole proton spectra as the temperature increases are given in Figure S3. (b) Table of the epoxy conversion percentage calculated from NMR signal integration. The reported percentages are the averages of the values obtained by the integration of the two NMR signals, and the error is the standard deviation. (c) Graph of TGPh epoxy conversion as a function of the temperature. The red line corresponds to the linear fitting.

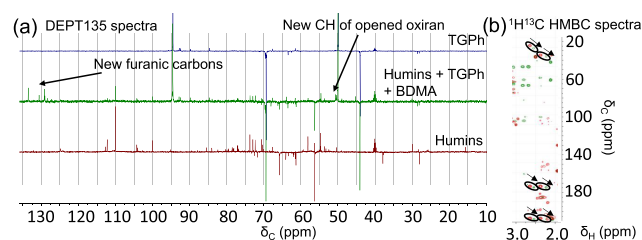


**Figure 15.** (a) DEPT135 of TGPh (blue); humins, TGPh, and BDMA (green); and humins alone (maroon). (b) Carbonyl region extracted from overlapped  $^1\text{H}$ - $^{13}\text{C}$  HMBC spectra of humins (red) and humins, TGPh, and BDMA at 60 °C (green). The whole spectra are given in Figure S4.

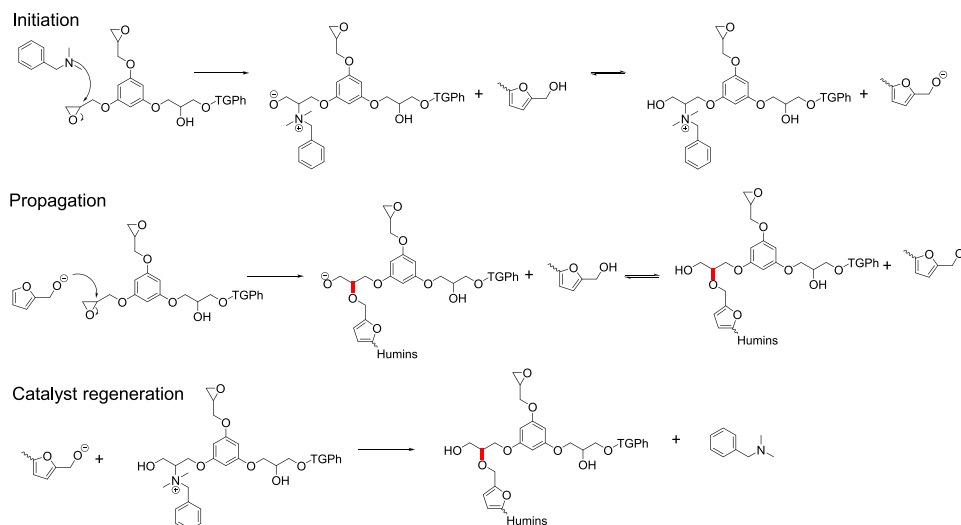
**Copolymerization of Humins and Triglycidyl Ether of Phloroglucinol in the Presence of the Accelerator.** When the cross-linking reaction was conducted in the presence of the accelerator, the appearance of new furanic species did not occur (Figure 17a). However, a decrease in TGPh epoxy proton signals still occurred (Figure 17b). The conversion reached 40%

at 90 °C (Figure 17c) as with BDMA, even if its trend as the temperature increased was not linear but quadratic (Figure 17d). The inspection of the HSQC spectrum showed two new  $-\text{CH}_2-$  peaks at  $\delta_{\text{H}} = 2.35$  and 2.28 ppm and at  $\delta_{\text{C}} = 62.7$  ppm (Figure 18a). As evidenced by the HMBC spectrum, these signals are coupled with the *N*-methyl groups of the accelerator (Figure 18a). A possible explanation is related to the opening of the TGPh oxirane ring by the hydroxyl group of the accelerator (Figure 18b).

This is consistent with the decrease in the epoxy signals and with the upfield shift of accelerator methylene protons experiencing a higher electron density, which reduces the effective field felt by the nuclei, leading to additional shielding. The predominance of this opening route at the temperatures explored on the one observed with BDMA reflects the higher diffusion rate of a small molecule like the accelerator with respect to humins, which allows an easier access of the accelerator to TGPh epoxides. As with BDMA, by increasing the temperature, the carbonyl signals become less intense (Figure S6). Another common feature is the decrease of the accelerator signals (Figure S6). From the evidence described so far, it is not possible to infer any information about hetero-cross-linking between humins and TGPh in the presence of the accelerator. As can be noticed in the DSC graph (Figure 3), in the presence of the accelerator, the reaction occurs in two consecutive steps. NMR results suggest that the first one involves TGPh epoxy ring opening by the accelerator. It is likely that this first step is followed by the reaction between humins and TGPh, but the insolubility of the cured material above 90 °C restricts the NMR temperature range accessibility.

**Copolymerization of Humins and Triglycidyl Ether of Phloroglucinol in the Presence of BDMA and the Accelerator.** The presence of both BDMA and the accelerator elicits the occurrence of both the features observed with BDMA and the accelerator alone, i.e., new furanic species originated by the humin hydroxyl nucleophilic attack to the TGPh oxirane ring and the accelerator TGPh ring opening, respectively (Figure 19a). This is in agreement with DSC data. The overall epoxy conversion estimated by the intensity decrease of proton signals (Figure 19b) was between 25 and 27% (Figure 19c) at the temperatures explored (60–80 °C), and the trend appeared to be mainly

#### Scheme 8. Proposed Mechanism for Humin and TGPh Cross-Linking<sup>a</sup>



<sup>a</sup>The new TGPh–humin bonds are colored in red.

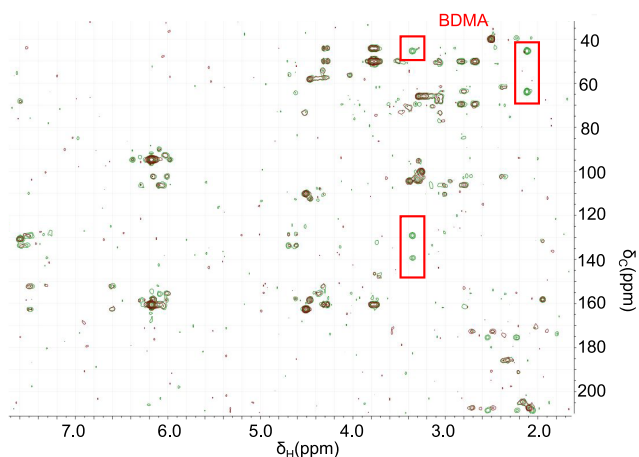


**Figure 16.** Superimposed  $^1\text{H}$ – $^{13}\text{C}$  HMBC spectra of humins, TGPh, and BDMA at 60 °C (green) and at 90 °C (maroon). Red boxes underline BDMA signals that disappear by increasing the temperature.

quadratic as with the accelerator (Figure 19d). These values are lower compared to the ones found with BDMA and the accelerator alone, suggesting an initial competition between the two epoxy opening routes rather than a cooperation.

The evolution of carbonyl signals was different with respect to the one observed with BDMA and the accelerator alone. The intensity of  $\gamma$ -dicarbonyl systems was very low at 60 °C (Figure S8), and then it increased upon increasing the temperature, especially for the  $\gamma$ -keto ester (Figure 20), consistently with the carbonyl content increase found in IR (Figure 9c). This strange trend can be explained considering only an initial higher level of system cyclization due to the presence of both the catalysts. Then, as the temperature increases, the esterification reaction becomes more recurrent, reversing the cyclization reactions and shifting the equilibria toward the carbonyl species (Scheme 9).

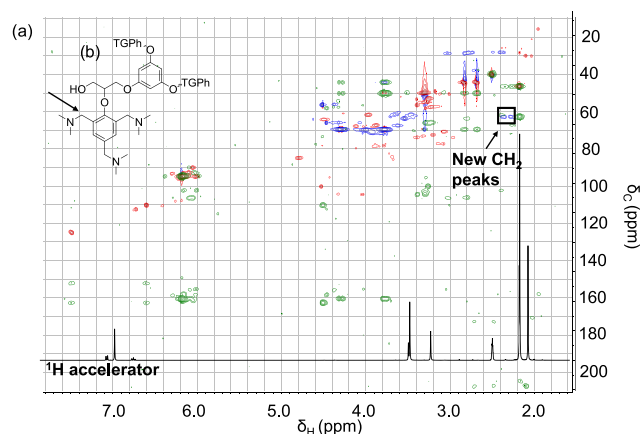


**Figure 18.** (a) Superimposition of the multiplicity-edited  $^1\text{H}$ – $^{13}\text{C}$  HSQC spectrum (positive peaks in red and negative in blue);  $^1\text{H}$ – $^{13}\text{C}$  HMBC spectrum (green) of humins, TGPh, and the accelerator mixture at 60 °C; and  $^1\text{H}$  spectrum of the accelerator. The new  $\text{CH}_2$  peaks are boxed in black. (b) Structure of the fragment generated by the opening of the TGPh epoxy ring by the accelerator. The arrow indicates the protons responsible for the new peaks in the HSQC spectrum.

## CONCLUSIONS

Humins are new promising materials to build biobased thermosets. However, the complexity of their structure makes the investigation of the structural changes that they undergo during their valorization much challenging. In this work, we demonstrated that humins can copolymerize with another biobased epoxy resin, namely, triglycidyl ether of phloroglucinol, through ether bond formation. The thermomechanical properties of the as-obtained materials will be discussed in a future publication. We found that in the presence of BDMA the cross-linking happens through the TGPh epoxy ring opening by the nucleophilic attack of the humin hydroxyl. An anionic polymerization mechanism catalyzed by the tertiary amine has

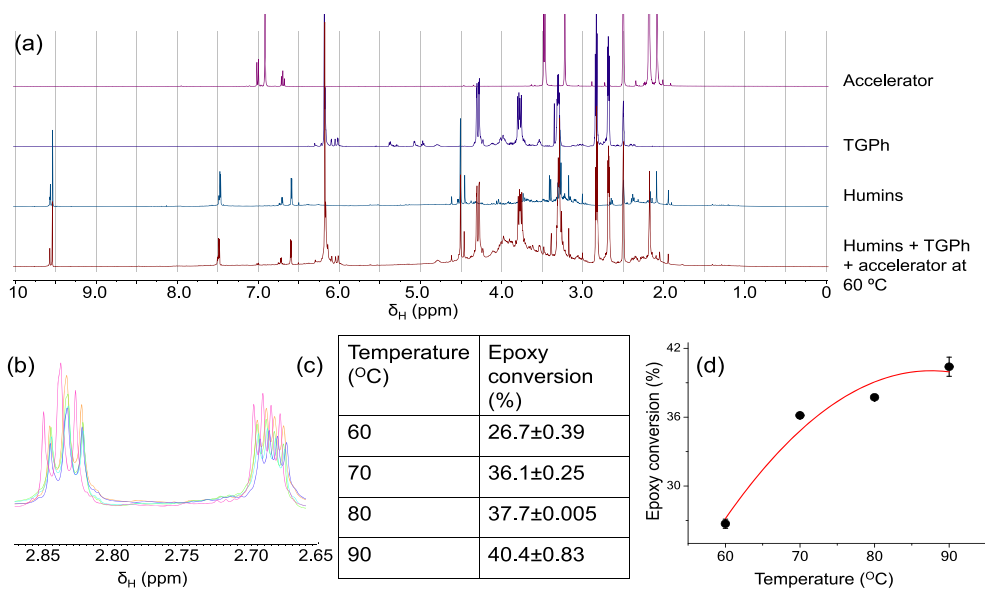


**Figure 17.** (a) Stacked  $^1\text{H}$  NMR spectra of the accelerator (purple), TGPh (violet), humins (petrol), and the mixture of all at 60 °C (maroon). (b) Enlargement of TGPh H5 epoxy peaks at increasing temperature: TGPh in pink; TGPh with humins and the accelerator at 60 °C in orange, at 70 °C in green, at 80 °C in cyan, and at 90 °C in blue. For the whole proton spectra as the temperature increases, see Figure S5. (c) Table of the TGPh epoxy conversion percentage calculated from the NMR signal integration. The reported percentages are the averages of the values obtained by the integration of the two NMR signals, and the error is the standard deviation. (d) Graph of TGPh epoxy conversion as a function of the temperature. The red line corresponds to the quadratic fitting.

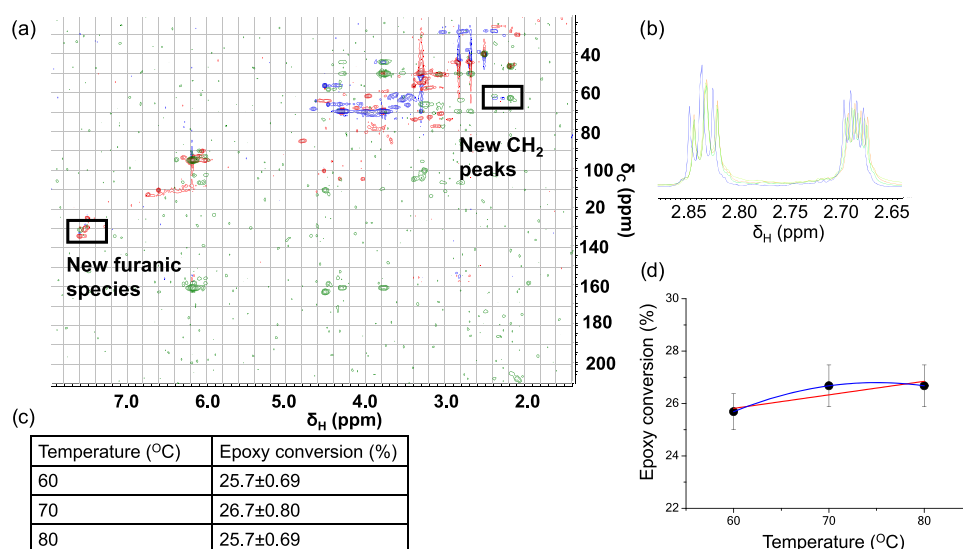


**Figure 19.** (a) Superimposition of the multiplicity-edited  $^1\text{H}$ - $^{13}\text{C}$  HSQC spectrum (positive peaks in red and negative in blue) and  $^1\text{H}$ - $^{13}\text{C}$  HMBC spectrum (green) of humins, TGPh, BDMA, and the accelerator mixture at 60 °C. (b) Enlargement of H5 epoxy peaks at increasing temperature: TGPh in blue; TGPh with humins and the accelerator at 60 °C in orange, at 70 °C in green, and at 80 °C in cyan. For the whole proton spectra as the temperature increases, see Figure S7. (c) Table of the epoxy conversion percentage calculated from the NMR signal integration. The reported percentages are the averages of the values obtained by the integration of the two NMR signals, and the error is the standard deviation. (d) Graph of TGPh epoxy conversion as a function of the temperature. The red line corresponds to the linear fitting and the blue one to the quadratic fitting.

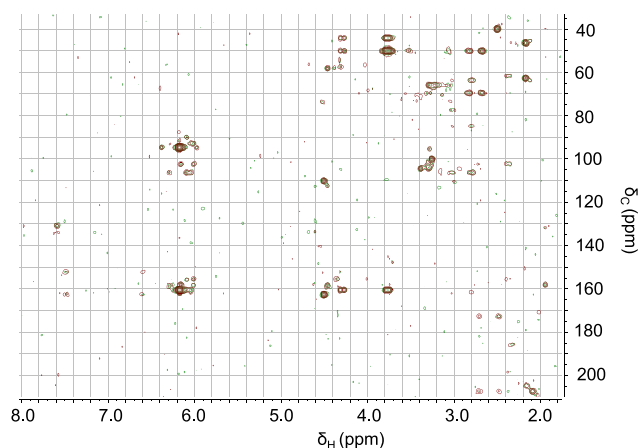


**Figure 20.** Superimposed  $^1\text{H}$ - $^{13}\text{C}$  HMBC spectra of humins, TGPh, BDMA, and the accelerator at 60 °C (green) and at 80 °C (maroon).

been proposed. Instead, when a competing nucleophile with a much higher mobility like the accelerator is present, the proofs of copolymerization are more subtle to highlight at the low temperature used for NMR experiments. Besides the reactivity toward triglycidyl ether of phloroglucinol, humins show a rearrangement of their furanic structure in which the carbonyl moieties play a leading role, especially the  $\gamma$ -dicarbonyl systems. Different reaction paths have been examined, and none of them revealed to be able to fully justify all of the complex spectral variations observed. It is likely that all of these reactions are concomitant; some of them could be reversible (e.g., esterification

and cyclization) and they compete. The predominance of one reaction on another revealed to be affected to a large extent by the specific reaction conditions. This work contributes to the elucidation of the structure of industrial humins, showing that they differ from laboratory-prepared humins, and to highlight the more reactive functional groups proposing different reaction pathways. A definitive reactivity pattern of humins is difficult to be established, mainly because of their intrinsic structural complexity and heterogeneity.

## ■ ASSOCIATED CONTENT

### Supporting Information

The Supporting Information is available free of charge on the ACS Publications website at DOI: 10.1021/acs.biomac.9b01248.

Two-dimensional NMR spectra of humins, TGPh, and their mixtures with BDMA and the accelerator; proton NMR spectra at increasing temperature of the mixtures (humins, TGPh, and catalysts) (PDF)

## ■ AUTHOR INFORMATION

### Corresponding Author

\*E-mail: [alice.mija@univ-cotedazur.fr](mailto:alice.mija@univ-cotedazur.fr).

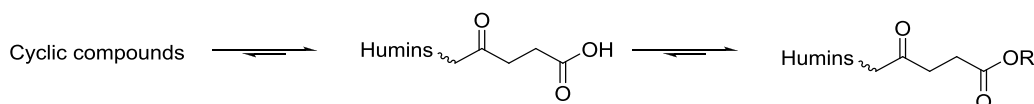
### ORCID

Alice Mija: 0000-0001-5208-5956

### Author Contributions

The manuscript was written by C.C. and A.M. R.D. did DSC experiments, and all of the other experiments were performed and analyzed by C.C. All authors have given approval to the final version of the manuscript.

## Scheme 9. Competing $\gamma$ -Keto Acid Reactions in the Presence of Both BDMA and the Accelerator: As the Temperature Increases, the Esterification Path Prevails on the Cyclization Reactions



## Funding

Funding for this work was received from the European Union's Horizon 2020 Research and Innovation program under Grant Agreement 723268 on a project KaRMA2020.

## Notes

The authors declare no competing financial interest.

## REFERENCES

- (1) Gandini, A. Polymers from Renewable Resources: A Challenge for the Future of Macromolecular Materials. *Macromolecules* **2008**, *41*, 9491–9504.
- (2) Isikgor, F. H.; Becer, C. R. Lignocellulosic Biomass: A Sustainable Platform for the Production of Bio-Based Chemicals and Polymers. *Polym. Chem.* **2015**, *6*, 4497–4559.
- (3) Mascal, M.; Nikitin, E. B. Direct, High-Yield Conversion of Cellulose into Biofuel. *Angew. Chem., Int. Ed.* **2008**, *47*, 7924–7926.
- (4) Binder, J. B.; Raines, R. T. Simple Chemical Transformation of Lignocellulosic Biomass into Furans for Fuels and Chemicals. *J. Am. Chem. Soc.* **2009**, *131*, 1979–1985.
- (5) Pin, J.-M.; Guigo, N.; Mija, A.; Vincent, L.; Sbirrazzuoli, N.; van der Waal, J. C.; de Jong, E. Valorization of Biorefinery Side-Stream Products: Combination of Humins with Polyfurfuryl Alcohol for Composite Elaboration. *ACS Sustainable Chem. Eng.* **2014**, *2*, 2182–2190.
- (6) Mija, A.; van der Waal, J. C.; Pin, J.-M.; Guigo, N.; de Jong, E. Humins as Promising Material for Producing Sustainable Carbohydrate-Derived Building Materials. *Constr. Build. Mater.* **2017**, *139*, 594–601.
- (7) Tosi, P.; van Klink, G. P. M.; Celzard, A.; Fierro, V.; Vincent, L.; de Jong, E.; Mija, A. Auto-Crosslinked Rigid Foams Derived from Biorefinery Byproducts. *ChemSusChem* **2018**, *11*, 2797–2809.
- (8) Filiciotto, L.; Balu, A. M.; Romero, A. A.; Rodríguez-Castellón, E.; van der Waal, J. C.; Luque, R. Benign-by-Design Preparation of Humin-Based Iron Oxide Catalytic Nanocomposites. *Green Chem.* **2017**, *19*, 4423–4434.
- (9) Schweizer, A. Caramel and Humin. A Contribution to the Knowledge of the Decomposition Products of Sugars. *Recl. Trav. Chim. Pays-Bas* **1938**, *57*, 345–382.
- (10) Schweizer, A. The Composition of the Humins Produced by the Action of Sulphuric Acid on Some Organic Substances. *Recl. Trav. Chim. Pays-Bas* **1940**, *59*, 781–784.
- (11) Horvat, J.; Klaić, B.; Metelko, B.; Šunjić, V. Mechanism of Levulinic Acid Formation. *Tetrahedron Lett.* **1985**, *26*, 2111–2114.
- (12) Girisuta, B.; Janssen, L. P. B. M.; Heeres, H. J. Kinetic Study on the Acid-Catalyzed Hydrolysis of Cellulose to Levulinic Acid. *Ind. Eng. Chem. Res.* **2007**, *46*, 1696–1708.
- (13) Filiciotto, L.; de Miguel, G.; Balu, A. M.; Romero, A. A.; van der Waal, J. C.; Luque, R. Towards the Photophysical Studies of Humin By-Products. *Chem. Commun.* **2017**, *53*, 7015–7017.
- (14) Summerskii, I. V.; Krutov, S. M.; Zarubin, M. Y. Humin-like Substances Formed under the Conditions of Industrial Hydrolysis of Wood. *Russ. J. Appl. Chem.* **2010**, *83*, 320–327.
- (15) Patil, S. K. R.; Lund, C. R. F. Formation and Growth of Humins via Aldol Addition and Condensation during Acid-Catalyzed Conversion of 5-Hydroxymethylfurfural. *Energy Fuels* **2011**, *25*, 4745–4755.
- (16) van Zandvoort, I.; Koers, E. J.; Weingarh, M.; Bruijninx, P. C. A.; Baldus, M.; Weckhuysen, B. M. Structural Characterization of <sup>13</sup>C-Enriched Humins and Alkali-Treated <sup>13</sup>C Humins by 2D Solid-State NMR. *Green Chem.* **2015**, *17*, 4383–4392.
- (17) Patil, S. K. R.; Heltzel, J.; Lund, C. R. F. Comparison of Structural Features of Humins Formed Catalytically from Glucose, Fructose, and 5-Hydroxymethylfurfuraldehyde. *Energy Fuels* **2012**, *26*, 5281–5293.
- (18) Constant, S.; Lancefield, C. S.; Weckhuysen, B. M.; Bruijninx, P. C. A. Quantification and Classification of Carbonyls in Industrial Humins and Lignins by <sup>19</sup>F NMR. *ACS Sustainable Chem. Eng.* **2017**, *5*, 965–972.
- (19) Titirici, M. M.; Thomas, A.; Yu, S.-H.; Müller, J.-O.; Antonietti, M. A Direct Synthesis of Mesoporous Carbons with Bicontinuous Pore Morphology from Crude Plant Material by Hydrothermal Carbonization. *Chem. Mater.* **2007**, *19*, 4205–4212.
- (20) Titirici, M.-M.; White, R. J.; Brun, N.; Budarin, V. L.; Su, D. S.; del Monte, F.; Clark, J. H.; MacLachlan, M. J. Sustainable Carbon Materials. *Chem. Soc. Rev.* **2015**, *44*, 250–290.
- (21) Sevilla, M.; Fuertes, A. B. The Production of Carbon Materials by Hydrothermal Carbonization of Cellulose. *Carbon* **2009**, *47*, 2281–2289.
- (22) Sevilla, M.; Fuertes, A. B. Chemical and Structural Properties of Carbonaceous Products Obtained by Hydrothermal Carbonization of Saccharides. *Chem. – Eur. J.* **2009**, *15*, 4195–4203.
- (23) Baccile, N.; Laurent, G.; Babonneau, F.; Fayon, F.; Titirici, M.-M.; Antonietti, M. Structural Characterization of Hydrothermal Carbon Spheres by Advanced Solid-State MAS <sup>13</sup>C NMR Investigations. *J. Phys. Chem. C* **2009**, *113*, 9644–9654.
- (24) Titirici, M.-M.; Antonietti, M. Chemistry and Materials Options of Sustainable Carbon Materials Made by Hydrothermal Carbonization. *Chem. Soc. Rev.* **2010**, *39*, 103–116.
- (25) Titirici, M.-M.; Antonietti, M.; Baccile, N. Hydrothermal Carbon from Biomass: A Comparison of the Local Structure from Poly- to Monosaccharides and Pentoses/Hexoses. *Green Chem.* **2008**, *10*, 1204–1212.
- (26) Falco, C.; Baccile, N.; Titirici, M.-M. Morphological and Structural Differences between Glucose, Cellulose and Lignocellulosic Biomass Derived Hydrothermal Carbons. *Green Chem.* **2011**, *13*, 3273–3281.
- (27) van Zandvoort, I.; Wang, Y.; Rasrendra, C. B.; van Eck, E. R. H.; Bruijninx, P. C. A.; Heeres, H. J.; Weckhuysen, B. M. Formation, Molecular Structure, and Morphology of Humins in Biomass Conversion: Influence of Feedstock and Processing Conditions. *ChemSusChem* **2013**, *6*, 1745–1758.
- (28) Montero, L.; Herrero, M.; Ibáñez, E.; Cifuentes, A. Separation and Characterization of Phlorotannins from Brown Algae *Cystoseira Abies-Marina* by Comprehensive Two-Dimensional Liquid Chromatography. *Electrophoresis* **2014**, *35*, 1644–1651.
- (29) Vandenberg, L. N.; Hauser, R.; Marcus, M.; Olea, N.; Welshons, W. V. Human Exposure to Bisphenol A (BPA). *Reprod. Toxicol.* **2007**, *24*, 139–177.
- (30) vom Saal, F. S.; Akingbemi, B. T.; Belcher, S. M.; Birnbaum, L. S.; Crain, D. A.; Eriksen, M.; Farabolini, F.; Guillette, L. J.; Hauser, R.; Heindel, J. J.; Ho, S. M.; Hunt, P. A.; Iguchi, T.; Jobling, S.; Kanno, J.; Kerl, R. A.; Knudsen, K. E.; Laufer, H.; LeBlanc, G. A.; Marcus, M.; McLachlan, J. A.; Myers, J. P.; Nadal, A.; Newbold, R. R.; Olea, N.; Prins, G. S.; Richter, C. A.; Rubin, B. S.; Sonnenschein, C.; Soto, A. M.; Talsness, C. E.; Vandenberg, J. G.; Vandenberg, L. N.; Walsler-Kuntz, D. R.; Watson, C. S.; Welshons, W. V.; Wetherill, Y.; Zoeller, R. T. Chapel Hill Bisphenol A Expert Panel Consensus Statement: Integration of Mechanisms, Effects in Animals and Potential to Impact Human Health at Current Levels of Exposure. *Reprod. Toxicol.* **2007**, *24*, 131–138.
- (31) Calafat, A. M.; Ye, X.; Wong, L.-Y.; Reidy, J. A.; Needham, L. L. Exposure of the U.S. Population to Bisphenol A and 4-Tertiary-Octylphenol: 2003–2004. *Environ. Health Perspect.* **2008**, *116*, 39–44.
- (32) Okada, H.; Tokunaga, T.; Liu, X.; Takayanagi, S.; Matsushima, A.; Shimohigashi, Y. Direct Evidence Revealing Structural Elements Essential for the High Binding Ability of Bisphenol A to Human Estrogen-Related Receptor-Gamma. *Environ. Health Perspect.* **2008**, *116*, 32–38.
- (33) Rozenberg, B. A. Kinetics, Thermodynamics and Mechanism of Reactions of Epoxy Oligomers with Amines. In *Epoxy Resins and Composites II*; Dušek, K., Ed.; Advances in Polymer Science; Springer: Berlin, Heidelberg, 1986; pp 113–165.
- (34) Han, J. L.; Hsieh, K. H.; Chiu, W. Y. Kinetics of Curing Reaction of Epoxide Catalyzed by Tertiary Amine. *J. Appl. Polym. Sci.* **1993**, *50*, 1099–1106.
- (35) Vazquez, A.; Bentaleb, D.; Williams, R. J. J. Curing of Diepoxides with Tertiary Amines: Influence of Temperature and Initiator

Concentration on Polymerization Rate and Glass Transition Temperature. *J. Appl. Polym. Sci.* **1991**, *43*, 967–976.

(36) Bowen, D. O.; Whiteside, R. C. Effect of Hydroxyl Compounds on Reactivity of Epoxy Resins. *Adv. Chem.* **1970**, *5*, 48–59.

(37) Gao, Y.; Yu, Y. The Synergistic Effect of Dicyandiamide and Resorcinol in the Curing of Epoxy Resins. *J. Appl. Polym. Sci.* **2003**, *89*, 1869–1874.

(38) Nouailhas, H.; Aouf, C.; Guerneve, C. L.; Caillol, S.; Boutevin, B.; Fulcrand, H. Synthesis and Properties of Biobased Epoxy Resins. Part 1. Glycidylation of Flavonoids by Epichlorohydrin. *J. Polym. Sci., Part A: Polym. Chem.* **2011**, *49*, 2261–2270.

(39) Noè, C.; Malburet, S.; Bouvet-Marchand, A.; Graillet, A.; Loubat, C.; Sangermano, M. Cationic Photopolymerization of Bio-Renewable Epoxidized Monomers. *Prog. Org. Coat.* **2019**, *133*, 131–138.

(40) Wu, L.; Moteki, T.; Gokhale, A. A.; Flaherty, D. W.; Toste, F. D. Production of Fuels and Chemicals from Biomass: Condensation Reactions and Beyond. *Chem* **2016**, *1*, 32–58.

(41) Woo, K. S.; Kim, H. Y.; Hwang, I. G.; Lee, S. H.; Jeong, H. S. Characteristics of the Thermal Degradation of Glucose and Maltose Solutions. *Prev. Nutr. Food Sci.* **2015**, *20*, 102–109.

(42) Faba, L.; Díaz, E.; Ordóñez, S. Base-Catalyzed Condensation of Levulinic Acid: A New Biorefinery Upgrading Approach. *ChemCatChem* **2016**, *8*, 1490–1494.